Title: Harnessing the regenerative potential of *interleukin11* to enhance heart repair

Authors: Kwangdeok Shin[1], Anjelica Rodriguez-Parks[1], Yu Xia[3], Chenyang Dong[4], Sunduz Kelles[4], Jingli Cao[3], Junsu Kang[1,2]

Affiliations

[1]Department of Cell and Regenerative Biology, School of Medicine and Public Health, University of Wisconsin - Madison, Madison, WI, 53705, USA.

[2]UW Carbone Cancer Center, School of Medicine and Public Health, University of Wisconsin - Madison, Madison, WI, 53705, USA

[3]Cardiovascular Research Institute, Department of Cell and Developmental Biology, Weill Cornell Medical College, New York, NY, 10065, USA.

[4]Departments of Statistics and of Biostatistics and Medical Informatics, University of Wisconsin - Madison, Madison, WI 53706, USA.

Abstract

Balancing between regenerative processes and fibrosis is crucial for heart repair[1]. However, strategies to regulate the balance between these two process are a barrier to the development of effective therapies for heart regeneration. While Interleukin 11 (IL11) is known as a fibrotic factor for the heart[2-4], its contribution to heart regeneration remains poorly understood. Here, we uncovered that *il11a* can initiate robust regenerative programs in the zebrafish heart, including cell cycle reentry of cardiomyocytes (CMs) and coronary expansion, even in the absence of injury. However, the prolonged *il11a* induction in uninjured hearts causes persistent fibroblast emergence, resulting in cardiac fibrosis. While deciphering the regenerative and fibrotic effects, we found that *il11*-dependent fibrosis, but not *il11*-dependent regeneration, is mediated through ERK activity, implying that the dual effects of *il11a* on regeneration and fibrosis can be uncoupled. To harness the regenerative ability of *il11a* for injured hearts, we devised a combinatorial treatment through *il11a* induction with ERK inhibition. Using this approach, we observed enhanced CM proliferation with mitigated fibrosis, achieving a balance between stimulating regenerative processes and curbing fibrotic outcomes. Thus, our findings unveil the mechanistic insights into regenerative roles of *il11* signaling, offering the potential therapeutic avenues that utilizes a paracrine regenerative factor to foster cardiac repair without exacerbating the fibrotic responses.

Introduction

Unlike adult mammals, adult zebrafish possess the remarkable capacity to regenerate lost cardiac tissues upon injury [5,6]. This regenerative ability of cardiac muscle cells can be achieved by dedifferentiation and proliferation of pre-existing CMs [7-9]. The regenerative events in CMs are orchestrated by molecular signals provided by activated non-muscular cells, including epicardium, endocardium, and immune cells, which create a regenerative niche [7,10-15]. Furthermore, similar to injured mammalian hearts, zebrafish exhibit an acute response to cardiac injury by forming fibrotic tissue at the injury site [16]. Although fibrosis is generally considered detrimental to regeneration, cardiac fibrosis is a double-edged event for heart regeneration as it plays a critical function to prevent rupture during the early phase of heart regeneration [16-18]. Indeed, preventing fibrosis during the early phase of the injured zebrafish hearts leads to defective heart repair [16]. In opposition to mammals, the cardiac fibrotic tissue in zebrafish hearts transiently form and are eventually replaced by newly formed CMs [19,20]. Therefore, dissecting the key signaling pathways governing regeneration and fibrosis is vital to understand the intricate processes of heart regeneration.

Results

Dynamics of endogenous *il11a* expression during zebrafish heart regeneration

Interleukin-11 (IL-11), a pleiotropic cytokine of the IL-6 family, plays regenerative roles in multiple injury contexts [21-23]. To investigate roles of *il11a*, one of two *il11* zebrafish homologs, in zebrafish hearts, we analyzed its expression with a newly created knock-in reporter line, *il11a*^{EGFP} **(Fig. 1A, B and Fig. S1A).** *il11a*^{EGFP} expression is undetectable in

uninjured hearts of embryonic and adult hearts **(Fig. 1A, B and Fig. S1B)**, suggesting its minimal contribution to heart development and homeostasis. Upon cardiac injury, *il11a* is robustly induced from non-CMs, primarily epicardium and endocardium **(Fig. 1A-D and Fig. S1B and C)**. *il11a*^{EGFP} expression was detectable as early as 1 dpa, highly and widely induced at 3 dpa throughout the ventricle, became localized to the wound site at 7 dpa, and largely undetectable by 14 dpa **(Fig. 1A, B)**. The robust and prompt *il11a*^{EGFP} expression throughout the ventricle during the early phase of regeneration suggests its potential influence on the activation of non-CMs, whereas wound-restricted *il11a*^{EGFP} expression during the mid-phase of regeneration indicates a potential interaction between *il11a* signaling and CMs for their renewal. The diminished expression of *il11a* by 14 dpa indicates the minimal contribution of *il11a* during the late phase of regeneration (**Fig. S1D, and E)**.

Mitogenic effects of *il11a* on cardiomyocytes in uninjured hearts

Previous studies of *il11* signaling in zebrafish hearts mainly focused on loss-of-function experiments with mutants of *il11* signaling components, such as *il11ra*, revealing impaired regeneration in the mutant hearts [24]. In rodents, *Il11* roles on cardiac fibrosis have been reported, but its regenerative roles remain unclear [2-4]. To our knowledge, there has been no comprehensive analysis of *il11* functionality on cell cycle reentry of CMs. To address this, we developed a new transgenic line*, Tg(actb2:loxp-BFP-STOP-loxp-il11a*), or *actb2:BS-il11a*, which allowed conditional overexpression (OE) of *il11a* in combination with *CreER* line. Crossing with *cmlc2:CreER*, we induced *il11a*OE from cardiac muscle cells upon tamoxifen treatment in the absece of injury **(Fig. 2A)**. Strikingly, *il11a*OE led to

the marked induction of CM proliferation in the uninjured hearts, whereas control hearts showed little to no proliferative CMs **(Fig. 2B, D),** providing evidence for the mitogenic roles of *il11a* on CMs. We next analyzed bulk RNA-seq profiles with control and *il11a*OE ventricles at 7 days post-treatment (dpt), identifying 1,327 genes (n = 862 and 465 for up- and down-regulated genes, respectively) with significantly changed expression levels (adjusted P [P-adj] < 0.05; fold change > 4) **(Fig. S2A and Supplementary Data 1).** *il11a*OE upregulated injury-inducible genes, including a regeneration-specific factor (*lepb)*, pro-regenerative ECM proteins (*fn1b* and *hmmr)*, injury-responsible transcription factor complex AP-1 components (*junba, fosl1a*), indicating activated regeneration response by *il11a* induction [25-28]. Gene ontology (GO) analyses with up-regulated genes in *il11a*OE hearts revealed enrichment in cell cycle, nuclear division, and DNA replication, highlighting active proliferation **(Fig. S2B)**. Additionally, gene set enrichment analysis (GSEA) identified significant enrichment of cell cycle signature in *il11a*OE **(Fig. S2C)**. *il11a* induction also highly upregulated key components of janus kinase/signal transducers and activators of transcription (JAK/STAT) signaling pathway, including *jak1, stat3*, and *socs3b,* which constitute a canonical downstream pathway of IL-11 [29-31] (**Fig. S2E**). Our *in situ* hybridization (ISH) analysis further confirmed that JAK/STAT-related factors are highly upregulated in CMs upon *il11a* induction, suggesting that JAK/STAT pathway is a major downstream effectors of *il11a* in CMs (**Fig. S2F**).

To re-enter cell cycle, CMs undergo dedifferentiation, characterized by sarcomere disassembly and downregulation of genes associated with mature CMs [8,32-34]. Indeed, the down-regulated genes in response to *il11a* induction are primarily associated with cardiac muscle contraction and metabolic processes **(Fig. S2B, D**), suggesting a transcriptional

shift from a mature to an immature state in CMs upon *il11a* induction. We next assessed the impact on sarcomere structure through α-actinin staining in control and *il11a*OE at 30 dpt. While control hearts displayed no sign of dedifferentiated CMs**,** *il11a*OE hearts exhibited a markedly increased sarcomere disassembly with blurred Z-discs **(Fig. 2C, E)**. To evaluate the long-term mitogenic effect of *il11a*OE, we analyzed the uninjured hearts at 3 and 7 months post-tamoxifen treatment (mpt). While no differences in body size and weight were observed between control and *il11a*OE **(Fig. S4)**, *il11a*OE hearts displayed a noticeable enlargement with a 20% increase in size at 3 mpt **(Fig. 2F, G)** and the significantly augmented size of the ventricles at 7 mpt **(Fig. 2F)**, a indicative of cardiomegaly.

Enlarged hearts can be caused by cardiac hypertrophy, a prominent mechanism responsible for the augmented mammalian hearts following injury [35], or hyperplasia, a desirable regenerative feature. To determine hypertrophic or hyperplastic effect of *il11a* induction, we quantified the CM density in the ventricles. The number of $Mef2^+$ nuclei in the ventricle significantly increased in *il11a*OE, compared to control (123.45 ± 8.71 and 107.45 ± 12.23 CMs/200μm^2 for *il11a*OE and control, respectively) **(Fig. 2H, I)**. Additionally, the individual CMs isolated from *il11a*OE hearts exhibited smaller length (83.65 ± 23.5 μm) than control (101.2 ± 23.2 μm) **(Fig. 2J, L)**. There is no notable difference in width between control and *il11a*OE CMs **(Fig. 2J, K)**. Collectively, these results demonstrate that *il11a* activation can bypass the injury signal to induce myocardial hyperplasia rather than hypertrophy, highlighting the mitogenic effect of *il11a* in zebrafish hearts.

***il11a* overexpression hypervascularizes the uninjured zebrafish hearts**

Stimulating revascularization of coronary vessels is a crucial regenerative process for the hearts [36-38]. To determine whether *il11a*OE can promote coronary vascularization in the absence of injury, we examined the coronary network using *fli1:EGFP*$^+$, which labels endothelial vessels [39,40]. Remarkably, whole-mount images demonstrated a more elaborate *fli1*:EGFP$^+$ coronary network in the *il11aOE* hearts as significantly increased vessel density was observed in *il11a*OE ventricles (18.84 ± 4.98% to 26.34% ± 3.27%) **(Fig. 3A, B)**. *fli1a*:EGFP$^+$ area in the cortical layer is also highly enhanced in *il11a*OE hearts (10.58 ± 1.19%), compared to control (6.78 ± 0.8%) **(Fig. 3C, D)**. Our transcriptome data revealed that *il11a*OE hearts exhibit a significant upregulation of genes associated with vascularization, including *angptl2a, emilin2a, hmmr, rspo3, sulf1,* and *thsd7aa* [37,41-45] **(Fig. S3A)**. Our single cell RNA sequencing (scRNA-seq) analysis with published dataset of regenerating hearts identified their injury-depedent induction predominantly within the epicardial cell clusters **(Fig. S3B-D)**. Given the pivotal role of the epicardium in guiding coronary growth [12,37,41,46], alongside with angiogenic factor increment by *il11a*, our data suggest that *il11a* induction activates epicardium to facilitate coronary growth.

While epicardium is normally quiescent in uninjured hearts, cardiac injury activates epicardium to undergo epithelial-to-mesenchymal transition (EMT) [47,48], giving rise to epicardial progenitor cells (EPCs), which are marked by *col12a1b* expression [49]. These *col12a1b*$^+$ EPCs subsequently differentiate into diverse epicardium-derived cells (EPDCs) in regenerating hearts [49]. We thus examined whether *il11a* induction can activate the dormant epicardium to initiate the generation of *col12a1b*$^+$ EPCs even in the

uninjured hearts. In control hearts, *tcf21*$^{+}$ epithelial cells are typically restricted to one or two layers outlining the ventricles (**Fig. 3E**). In contrast, within *il11a*OE hearts, *tcf21*$^{+}$ layers expanded into the mesenchymal layers, a deeper region of the cortical wall, indicating that *il11a* induction triggers the epicardium to undergo EMT **(Fig. 3E)**. Evidently, a subset of *tcf21*$^{+}$ epicardial cells within *il11a*OE hearts display *col12a1b:EGFP* expression at 10 dpt, indicating that *il11a* induction activates *tcf21*$^{+}$ epicardial cells to become EPCs (**Fig. 3E**). By 30 dpt, *il11a*OE hearts displayed extensive expansion of *col12a1b*$^{+}$ EPCs populations within the deeper mesenchymal layer (**Fig. 3E**). In contrast, *col12a1b*$^{+}$ EPCs were conspicuously absent in control hearts at 10 and 30 dpt. Our results indicate that *il11a* can stimulate the epicardium to generate EPCs which subsequently differentiate into EPDCs impacting coronary vascularization.

The fibrotic effects of prolonged *il11a* treatment

Given recent reports indicating IL-11 as a fibrotic factor [2-4], we explored whether *il11a* could exert a fibrotic role in zebrafish hearts. At 30 dpt, there is no significant difference of collagen deposition between control and *il11a*OE hearts **(Fig. 4A)**. While fibrotic tissue was undetectable in control hearts, *il11a*OE hearts exhibited collagen accumulation in the cortical layer at 3 mpt and massive collagen deposition at 7 mpt (**Fig. 4A, B**). The cardiac fibrosis mainly manifested in the cortical layer and surface, rather than within the ventricles, and its thickness expanded over time **(Fig. 4A, B)**, affirming fibrotic function of *il11* in zebrafish.

In regenerating zebrafish hearts, cardiac fibrosis is largely mediated by epicardium-derived fibroblasts that appear in the cortical layer following injury [10,16,50,51].

Given that the fibrosis driven by *il11a* is predominantly observed in this cortical layer, we hypothesize that prolonged *il11a* exposure might lead to fibrosis due to sustained cardiac fibroblast production from an activated epicardium. Supporting this notion, *il11a* induced the emergence of ACTA2^{+} cardiac fibroblasts in the cortical layer without an injury at 30 dpt (**Fig. 4C, D)**. As ERK, a downstream effector of the MAPK pathway, controls various cellular processes, including proliferation, survival, and fibrosis [52,53], we questioned whether ERK mediates *il11a*-inducible fibrosis in the epicardium. The phosphorylated ERK (pERK) signal, representing active ERK, was minimal in the *tcf21*$^{+}$ epicardium of the control hearts, but remarkably increased upon *il11a* induction (**Fig. 4E, F**). The pERK signal remained undetectable in CMs in both control and *il11a*OE (**Fig. S5**), indicating the limited impact of MAPK/ERK signaling on CM proliferation. These findings suggest that the persistent *il11a* induction can provoke fibrosis by promoting the presence of cardiac fibroblasts from MAPK/ERK-activated EPCs.

il11a induction with pERK inhibition can enhance CM proliferation without exacerbating fibrosis

Our studies on *il11a*OE in uninjured hearts demonstrated dual roles of *il11a,* acting as a double-edged sword in heart repair: *il11* signaling can promote the regenerative program while also contributing to cardiac fibrosis (**Fig. 4G**). We next explored whether this dual functionality of *il11a* is also operational in injured hearts. At 14 days post-injured hearts, ectopic *il11a* activation significantly increased CM proliferation (8.61 ± 1.26 % and 5.20 ± 0.80 % in OE and control, respectively) **(Fig. 5A, B and Fig. S6)**, confirming its mitogenic effect on injured hearts. To assess the fibrotic effects of *il11a* on injured hearts,

we performed ventricular apex resection with control and *il11a*OE fish and collected hearts at 30 dpa, at which myocardial wall regeneration is typically completed [5]. Control hearts had limited scarring at the wound, a sign of successful scar resolution (**Fig. 5C, D**). In contrast, *il11a*OE hearts exhibited apparent collagen-rich scar tissues at the injury site (8.19 ± 3.33 % and 0.62 ± 0.67 % in OE and control, respectively) (**Fig. 5C, D**). This time point is relatively earlier than when *il11a*-stimulated fibrosis is observed in the uninjured hearts, as uninjured *il11a*OE hearts did not display noticeable collagen-rich fibrotic tissues at 30 dpt (**Fig. 4A**). Furthermore, ectopic *il11a* induction led to the persistence of *col12a1b*$^{+}$ EPCs and fibrotic tissues at the injury site in cryoinjured hearts (**Fig. S7**). Hence, *il11a* induction gradually accumulates collagen in uninjured hearts, but its fibrotic function is accelerated in the presence of injury.

To harness the regenerative potential of *il11a* for injured hearts, mitigating its fibrotic function is crucial. Thus, we devised a concurrent treatment strategy involving *il11a* induction with preventing cardiac fibrosis through ERK/MAPK inhibition (**Fig. 5E**). This approach aims to facilitate heart repair by promoting CM proliferation via *il11a* induction while minimizing cardiac fibrosis by inhibiting fibrosis-specific signaling at a later time point. To achieve this, we administered U0126, an ERK inhibitor [54], for a month, starting at 2 weeks after cryoinjury with control and *il11a*OE fish and collected hearts at 45 days post-injury (dpi) (**Fig. 5F**). Collagen deposition was not evident in the hearts of control fish treated with vehicle or U0126 (**Fig. 5G, H**), suggesting that U0126 treatment during the late regenerative phase minimally affects heart repair. By contrast, *il11a*OE hearts treated with vehicle displayed significant collagen deposition at the injury site, confirming the fibrotic function of *il11a* in injured hearts (**Fig. 5G, H**). Interestingly, U0126

treatment in *il11a*OE significantly reduced the presence of fibrotic tissues at the injury site (**Fig. 5G, H**), implicating that inhibiting pERK reduces *il11a*-induced cardiac fibrosis. Moreover, we observed that CMs in *il11a*OE hearts treated with U0126 and vehicle exhibited a similar proliferation rate (**Fig. 5I, J**), highlighting the specific effect of ERK/MAPK inhibition on cardiac fibrosis. Taken together, our findings provide a proof-of-principle that combinatorial treatment of *il11a* induction with inhibiting fibrosis holds significant potential for enhancing heart regeneration following cardiac injury.

Discussion

Our expression analysis and functional assays shed light on that *il11* is a potent regenerative factor for heart regeneration. During normal heart regeneration, *il11a* is produced from non-CMs at the early phase to trigger regenerative programs by initiating cell cycle reentry for CMs, activating epicardium for generating EPCs, and stimulating vascularization. Its expression is decommissioned at the late regenerative phase to block aberrant outcomes, such as preventing fibrosis resolution. We demonstrate that *il11a* induction in the uninjured heart can bypass cardiac injury cues to stimulate regeneration programs, demonstrating that *il11* is a potent regenerative factor to enhance heart repair. In particular, we showed that *il11a* induction can enlarge hearts via CM hyperplasia rather than hypertrophy. However, prolonged activation of epicardium by *il11a* leads to the persistent presence of EPCs, resulting in the constant production of cardiac fibroblasts and subsequent fibrosis. Thus, our study demonsrate that IL-11 treatment should be tightly regulated for effective and successful heart regeneration.

Regenerative paracrine factors are promising therapeutic candidates, due to their

potential efficacy as drugs and simple delivery methods. Cytosolic and nuclear proteins require specific methodologies to be delivered inside the cells, presenting an additional challenge [55-57]. However, our studies reveal that application of paracrine factors for heart regeneration should be carefully considered, especially in the aspect of cardiac fibrosis. One essential yet paradoxical regenerative event is to accumulate ECM proteins, such as collagen, by cardiac fibroblasts at the injury site. Although this fibrotic response is thought to be detrimental due to its non-contratile feature potentially causing heart failure [58], it is indispensable and beneficial for heart regeneration at the early phase [16,59,60]. As demonstrated in our study, a single paracrine factor and signaling can target multiple cardiac cells, including CMs, endocardium/endothelium, and epicardium. Notably, the activated epicardial cells undergo reprogramming to generate progenitor cells, which later differentiate into the cardiac fibroblasts contributing to fibrosis. Consequently, a paracrine factor can serve as a double-edged sword to induce beneficial regenerative effects as well as detrimental cardiac fibrosis. In nature, these two effects are precisely balanced through tight spatiotemporal control during heart regeneration. However, current methodologies to enhance heart regeneration often face limitations, such as targeting multiple cell types by viral vectors or delivery vehicles [61], and obscure duration for functional recovery [62]. Here, we prove that delivering *il11a* paracrine factor, along with inhibiting cardiac fibrosis via ERK inhibitor treatment in injured hearts, can maintain CM proliferation without exacerbating fibrosis. Therefore, paracrine factor treatment combined with attenuating cardiac fibrosis can represent a more effective regenerative medicine strategy.

Previous works on *il11* across animal species and tissues have revealed

seemingly conflicting results, as *il11* is known to have both regenerative and fibrotic properties [2,3,21-24,30,63-67]. Regarding the hearts, antifibrotic/cardioprotective and fibrotic roles of *Il11* were reported [2,3,24,30,67]. Our study can explain these opposing results by highlighting pleiotrophic function of *il11*. Our study offers important new insights into IL-11 biology for cardiac regeneration and fibrosis. A deeper understanding of IL-11-associated cellular and molecular processes will be critical for developing a therapeutic strategy for precise regenerative effects with limited fibrosis.

Methods

Zebrafish

Wild-type or transgenic male and female zebrafish of the outbred Ekkwill (EK) strain ranging up to 18 months of age were used for all zebrafish experiments. The following transgenic lines were used in this study: *Tg(cmlc2:creER)*^{pd10}, *Tg(cmlc2:mCherry-N-2A-Fluc)*^{pd71}, *Tg(col12a1b:EGFP)*^{wcm108}, *Tg(fli1:EGFP)*^{y1}, *Tg(−6.5kdrl:mCherry)*^{ci5}, *Tg(tcf21:mCherry-NTR)*^{pd108} [8,49,68-71]. To generate *actb2:loxP-BFP-loxP-il11a* (*uwk28*), the transgenic construct was generated by modifying *actb2:loxP-BFP-loxP-nrg1* [72]. The *nrg1* sequence were replaced with *il11a* cDNA amplified by PCR using wild-type zebrafish cDNA libraries. Primers are listed in **Table S1**. The entire cassette was flanked with I-*Sce*I sites for meganusclease-enhanced transgenesis. The identified founder line was crossed with *cmlc2:creER* to induce *il11a* induction upon tamoxifen treatment. Water temperature was maintained at 26°C for animals unless otherwise indicated. Work with zebrafish was performed in accordance with University of Wisconsin-Madison guidelines. Partial ventricular resention surgery was performed as described previously [5], in which ~20% of the cardiac ventricle was removed at the apex. Ventricular cryoinjuries were performed as described [73]. Briefly, the ventricular wall was applied by a cryoprobe precooled in liquid nitrogen.

Generation of *il11a*^{EGFP}

To generate *il11a* knock-in reporter (*uwk25*), we generated a donor construct having 5' and 3' homology arms (HAs) and *EGFP-SV40pA* cassette. 5' and 3' HAs were amplified using genomic DNA extracted from fish that were used for injection. These HA fragments

were subcloned into the pCS2-EGFP-pA-IsceI vector. For linearization, sgRNA located in 3' HA ("GG ATC AAGTG TTACT CGCTC AGG") was used. sgRNAs synthesis and microinjection were described in [74]. Briefly, sgRNA were synthesized by a cloning-free method using the MEGAshortscript T7 Transcription Kit (Invitrogen, AM1354) and purified by the RNA purification Kit (Zymogen, R1016) according to the manufacturer's instructions. A sgRNA (25~30 ng/ul) and a donor plasmid (20-25 ng/ul) were mixed and co-injected with Cas9 protein (0.5ug/ul; PNABio, CP01) into the one-cell stage embryos. After injection, none of larvae exhibit EGFP expression without injury. To sort F_0 animals carrying *EGFP-pA* at the *il11a* locus, fin folds were amputated at 3 or 4 dpf, and embryos displaying EGFP fluorescence near the injury site at 1 dpa were selected. EGFP positive larvae were raised to adulthood, and founders were screened with F_1 progenies driving fin fold injury-inducible EGFP expression. Integration at the *il11a* locus was identified by PCR with primers described in **Table S1**, followed by Sanger sequencing. For expression pattern to determine spatiotemporal expression of *il11a*^{EGFP}, at least three biological replicates, unless indicated, were examined per each time point and per observation to allow for potential variability within a single experiment.

Immunostaining, histology and imaging

Hearts were fixed with 4% paraformaldehyde (PFA) for 1 hour at room temperature. Cryosectioning and immunohistochemistry were performed as described previously with modifications [25]. Hearts were cryosectioned at 10μm. Heart sections were equally distributed onto four to six serial slides so that each slide contained sections representing all area of the ventricle. 5 or 10% goat serum, 1% BSA, 1% DMSO, and 0.2% Triton X-

100 solution was used for blocking and antibody staining. The primary and secondary antibodies used in this study were: anti-myosin heavy chain (mouse, F59; Developmental Studies Hybridoma Bank; 1:50 or mouse, MF20; Developmental Studies Hybridoma Bank; 1:50), anti-EGFP (rabbit, A11122; Life Technologies; 1:200), anti-EGFP (chicken, GFP-1020; Aves Labs; 1:2000), anti-Ds-Red (rabbit, 632496; Clontech; 1:500), anti-mCherry (chicken, MC87977980; Aves Labs; 1:500), anti-Raldh2 (rabbit, GTX124302; Genetex; 1:200), anti-PCNA (mouse, P8825; Sigma; 1:200), anti-α-actinin (mouse, A7811; Sigma, 1:200), anti-ACTA2 (rabbit, GTX124505; GeneTex; 1:200), anti-pERK (rabbit, 9101; Cell Signaling Technology; 1:250). Anti-Mef2 (rabbit; 1:200) [49], Alexa Fluor 488 (mouse, rabbit, and chicken; A11029, A11034, and A11039; Life Technologies; 1:500), Alexa Fluor 594 (mouse and rabbit; A11032 and A11037; Life Technologies; 1:500). *In situ* hybridization (ISH) on cryosections of 4% paraformaldehyde-fixed hearts was performed as previously described [25]. To generate digoxigenin-labeled probes, we used cDNA for 3' part of each gene. Primer sequences are listed in **Table S1**. Images of cardiac tissue sections were acquired using an Eclipse Ti-U inverted compound microscope (Nikon) or BZ-X810 fluorescence microscope (Keyence). Images were processed using either NIS-Elements (Nikon), ZEN (Zeiss), BZ-X800 analyzer (Keyence) or FIJI/ImageJ software.

AFOG staining and quantification of collagen deposition

AFOG staining was performed on 10 μm sections as described[5]. Samples were first incubated at 60°C for 2 hr with Bouin preheated at 60°C for 30 min; slides were then rinsed in running water for 30 min, and incubated with phosphomolybdic acid solution,

followed by the sample incubation in AFGO staining solution for 10 min. For quantification of collagen deposition, collagen^{+} area was manually measured using ImageJ and normalized by the ventricular size and normalized by the entire ventricle size. Two to four largest sections were analyzed for each heart.

Drug treatment

For tamoxifen treatments, zebrafish were bathed in 5 μM tamoxifen (Sigma-Aldrich, T5648) for 24 hr. Zebrafish were rinsed with fresh aquarium water and returned to the recirculating water system for feeding. For 4-hydroxytamoxifen (4-HT) treatments, zebrafish were intraperitoneally injected with 10 μl of 3mM 4-HT (Sigma-Aldrich, H7904) for 4 consecutive days and returned to the water system as described previously [75]. For U0126 treatments, Fish were intraperitoneally injected with 10 μl of the 10 μM U0126 or 0.1 % DMSO in phosphate-buffered saline (PBS) using a 10 μl Hamilton syringe (1701SN) once daily for 30 days. CM ablation and imaging were performed as previously described in [76]. Briefly, 5 dpf *cmlc2:mCherry-NTR* zebrafish were incubated in 10 mM Metronidazole for 18 hours. The Mtz-containing medium was replaced with fresh embryo medium several times and larvae were returned to 28°C.

Whole mount imaging

Whole mount imaging was performed as described in [77]. Hearts were isolated from tricaine-anesthetized adult animals. Freshly isolated hearts were rinsed with 1X PBS and immediately mounted in 1% low-melting agarose/PBS (0.01% triance) in a glass bottom dish. The images were acquired using an Eclipse Ti-U inverted compound microscope

(Nikon). Confocal sections covering the entire heart were imaged from ventral sides and processed to obtain maximal intensity projections. *Fli1a:EGFP*$^{+}$ area within a ventricle was assessed using ImageJ/Fiji image to measure vascular density.

Quantification of ventricular size

Hearts were collected from tricaine-anesthetized adult animals and fixed with 4% PFA for 1 hour at room temperature. Hearts were rinsed with 1X PBS with 0.1% Tween-20 and aligned on specimen stage. The images were acquired using an Zeiss Axio Zoom.V16 fluorescence stereo microscope. For quantification of ventricular size, the size was measured as described in [32]. the ventricular outline was manually traced, and the area encompassed by the outline was quantified using ZEN microscopy software (Blue edition).

Quantification of cardiomyocyte size

The size of cardiomyocytes were quantified as previously described in [32]. Zebrafish ventricles were fixed in 3% PFA for 5 min and incubated in PBS supplemented with 1 mg/mL collagenase type 4 (Worthington Biochemical) at 4°C overnight. Dissociated cardiac muscle cells are deposited into a slide using a cytocentrifuge (Thermo Scientific, Cytospin 4), followed by immunofluorescence using an anti-α-actinin antibody. Images of α-actinin^{+} cells were acquired by BZ-X810 fluorescence microscope (Keyence) and used to measure the size of individual cardiomyocytes using FIJI/ImageJ software.

RNA isolation and bioinformatics

RNA was isolated from control and *il11a*OE hearts using Tri-Reagent (ThermoFisher). Complementary DNA (cDNA) was synthesized from 300 ng to 1 µg of total RNA using a NEB ProtoScript II first strand cDNA synthesis kit (NEB, E6560). For RNA-sequencing, total RNA was prepared from three biological replicate pools of 7 dpt uninjured heart samples of control and *il11a*OE transgenic fish. Generation of mRNA libraries and sequencing were performed at the Biotechnology center at UW-Madison using an Illumina NovaSeq with 150 bp paired-end runs. Sequences were aligned to the zebrafish genome (GRCz11) using HISAT2 [78]. Differentially regulated transcripts were identified using Featurecount [79] and Deseq2 [80]. GO-term and GSEA analyses were done by the enrichGo and gseGO functions of clusterProfiler [81]. Accession numbers for transcriptome data sets are GEO233833.

scRNA-seq analysis of uninjured and regenerating hearts was done as described in [82]. Briefly, we obtained count files from GSE159032 and GSE158919 [44] and reanalyzed with Seurat package [83]. Low quality cells (nFeature_RNA ≥ 4100, mitoRatio ≥ 0.25) were filtered out. The 50 principal components (PCs) of the PCA with resolution 4 were used for clustering. Marker genes to identify cell-types are listed in [82].

Quantification

Quantification of EGFP$^+$ area was performed using the FIJI/ImageJ software. 2-5 sections were used to determine the values in one cardiac sample. ROIs were determined by manual selection of heart outlines, with guidance provided by the red channel (MHC) images. To quantify EGFP$^+$, selected ROIs were converted to 8 bit, adjusted with threshold, which is determined by autofluorescence level of EGFP$^+$ areas in ROIs were

evaluated. For CM proliferation index, PCNA$^+$ Mef2$^+$ CMs were quantified from Mef2$^+$ CMs as described previously [15]. Images of the injury area were taken by 400 μm (W) x 200 μm (H) from the apical edge of the ventricular myocardium. The number of Mef2$^+$ PCNA$^+$ cells were manually counted using FIJI/ImageJ software. Three or four sections were analyzed for each heart. Quantification in uninjured hearts was conducted similarly, except that images of the mid-ventricular myocardium were taken for quantification. For quantification of sarcomere disorganization, images of α-actinin$^+$ area were randomly taken by 200 μm (W) x 200 μm (H) from the ventricular myocardium. The disorganized sarcomere area was manually measured and normalized by the entire α-actinin$^+$ area using FIJI/ImageJ software. For quantification of cardiomyocyte density, at least three area (200 μm (W) x 200 μm (H)) were randomly taken from the ventricular myocardium. The number of mef2$^+$ cells were manually counted using FIJI/ImageJ software. For quantification of pERK$^+$ area in tcf21:mCherry$^+$ area, ROIs were determined by red channel (mCherry) images and the green$^+$ (pERK) area in ROIs were evaluated.

Statistical values are represented as mean ± SD unless otherwise indicated. To determine the statistical significance, p values were caculated using unpaired t-tests unless otherwise indicated. p values are described in each figure legend.

Acknowledgments

We thank UW-Madison School of Medicine and Public Health (SMPH) BRMS (Biomedical Research Models Services) staffs for zebrafish care; the University of Wisconsin Biotechnology Center DNA Sequencing Facility (Research Resource Identifier – RRID:SCR_017759) for providing RNA-seq services; Seungwon Ryu and Isabella

Matahari Silaban for assistance with sample preparation; and Jeffery F. Dilworth for comments on the manuscript.

Competing interests

The authors declare that they have no competing interests.

Author contributions

Biological experiments: KS, AR, YX

Computational analysis and data curation: KS, CD, JK

Conceptualization: KS, JK

Writing original draft: KS, JK

Reviewing, Editing: KS, JK

Supervision: SK, JC, JK

Funding: JC, JK

Funding:

National Institutes of Health grant R35 GM 137878 (JK)

National Institutes of Health grant R01 HL 151522 (JK)

National Institutes of Health, University of Wisconsin Carbone Cancer Center Support grant P30 CA 014520 (JK)

University of Wisconsin Institute for Clinical and Translational Research (UW ICTR) pilot grant

National Institutes of Health grant R01 HL 155607 (JC)

National Institutes of Health grant R01 HL 166518 (JC)

Stem Cell and Regenerative Medicine Center Research Training Award (KS)

Data and materials availability: Sequencing data have been deposited in GEO under accession code GEO233833. Reviewer token is qtqrwaqwhxkvpin.

Figures and Figure legends

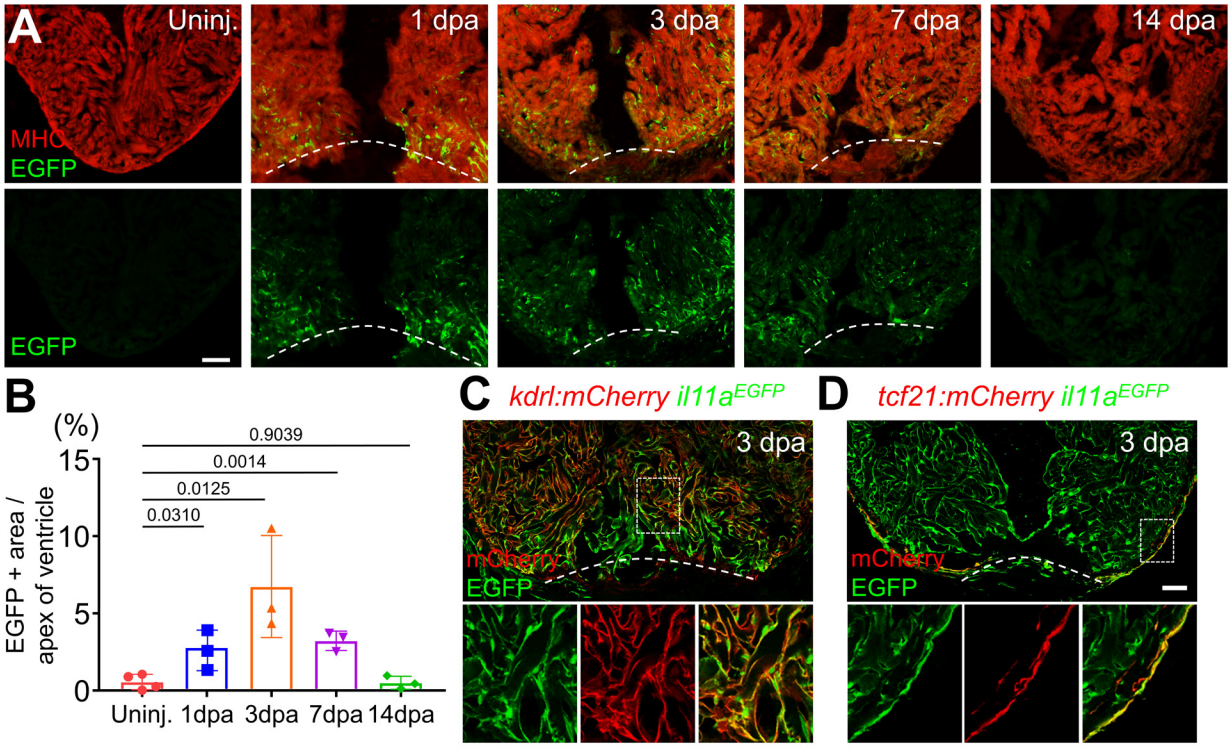

Figure 1. Spatiotemporal *il11a* expression during heart regeneration in adult zebrafish. (**A**) Representative cardiac section images of *il11a*^{EGFP}. dpa, days post-amputation. (**B**) Quantification of EGFP expression area near the wound area. n = 3 - 4. (**C, D**) Comparison of *il11a*^{EGFP} expressing cells with *kdrl:mCherry* (**C**) and *tcf21:mCherry* (**D**) in 3 dpa hearts. *kdrl:mCherry* and *tcf21:mCherry* represent endocardium and epicardium, respectively. Dash boxes correspond to the region magnified in below panels. Dotted lines demarcate the amputation plane. Scale bars, 100 μm in **A**, 50 μm in **D**.

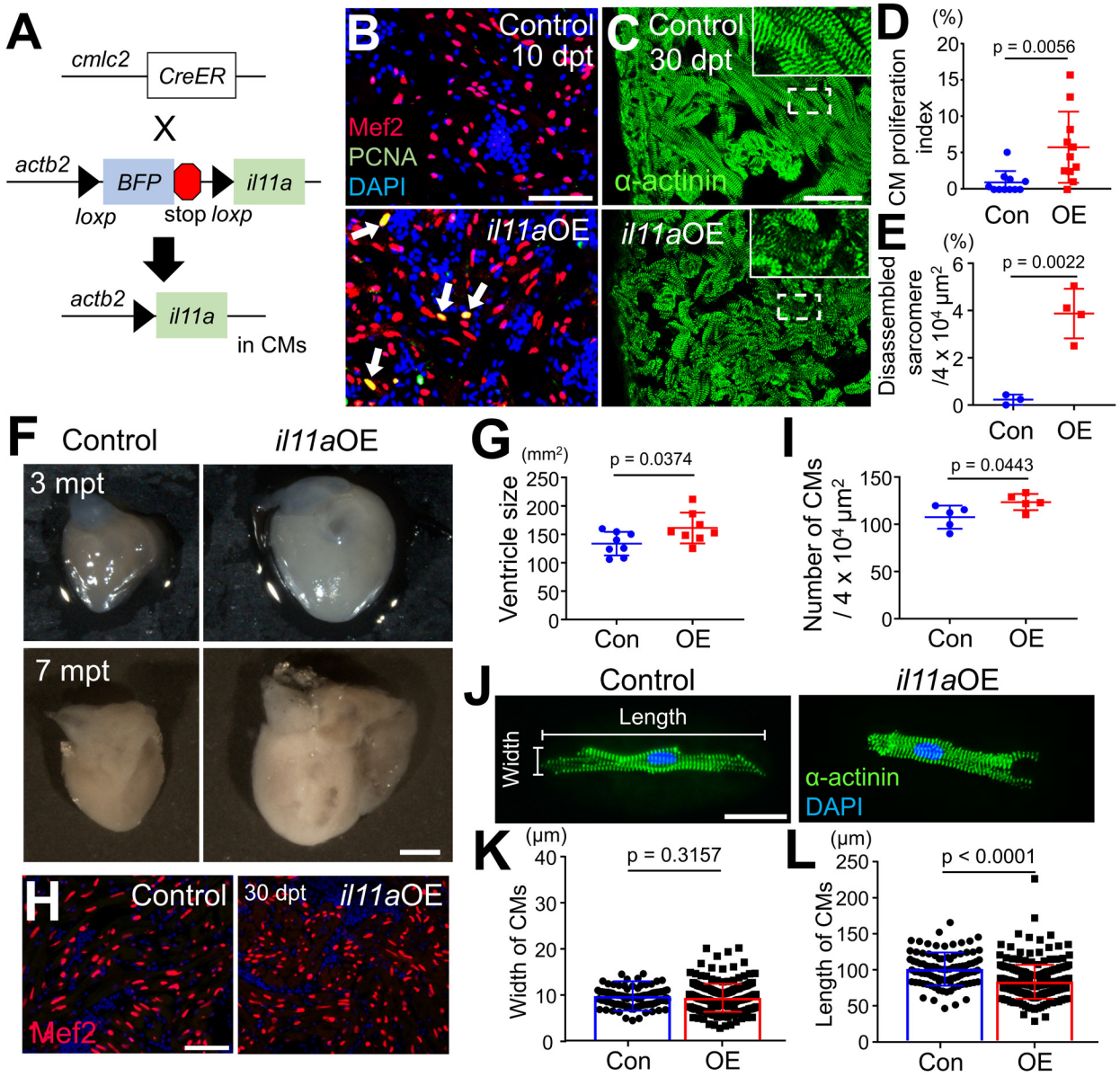

Figure 2. Myocardial *il11a* overexpression (OE) triggers CM proliferation in the absence of injury. (**A**) Schematic of tamoxifen (Tam) or 4-HT (4-Hydroxytamoxifen) inducible *il11a* overexpression (OE). *Tg*(*actb2:loxp-TagBFP-STOP-loxp-il11a)*; *cmlc2:CreER* were administered with Tam or 4-HT to overexpress *il11a* (*il11a*OE). *Cre*-negative littermates were used as control. (**B**) Representative cardiac section images stained with Mef2 (Red) and PCNA (Green) from control and *il11a*OE at 10 day post-

treatment (dpt). Arrows indicate proliferative CMs. (**C**) Representative cardiac sections images stained with α-antinin (green) from control and *il11a*OE uninjured hearts at 30 dpt. Insets correspond to higher magnifications of dashed boxes. (**D**) CM proliferation index of uninjured hearts of control (Con) and *il11a*OE (OE) at 7 dpt. n = 5. (**E**) Quantification of disorganized sarcomeric structures in the ventricles of control (Con) and *il11a*OE (OE) at 30 dpt. n = 3 - 4. (**F**) Whole-mount images of 3 and 7 month post-treatment (mpt) hearts from control and *il11a*OE. (**G**) Quantification of the ventricle size from 3 mpt control (Con) and *il11a*OE (OE). n = 8. (**H**) Representative cardiac section images of 30 dpt control and *il11a*OE stained with Mef2 (red) and DAPI (blue). (**I**) Quantification for CM numbers in the ventricles from 30 dpt control (Con) and *il11a*OE (OE). n = 5. (**J**) Representative images of dissociated ventricular CMs stained with α-antinin (green) from 2 mpt control and *il11a*OE. (**K**, **L**) Quantification of the width (**K**) and the length (**L**) of individual CMs. n = 92 for control (Con) and 234 for *il11a*OE (OE). Scale bars, 50 μm in **B, C** and **H**, 0.5 mm in **F**, 25 μm in **J**.

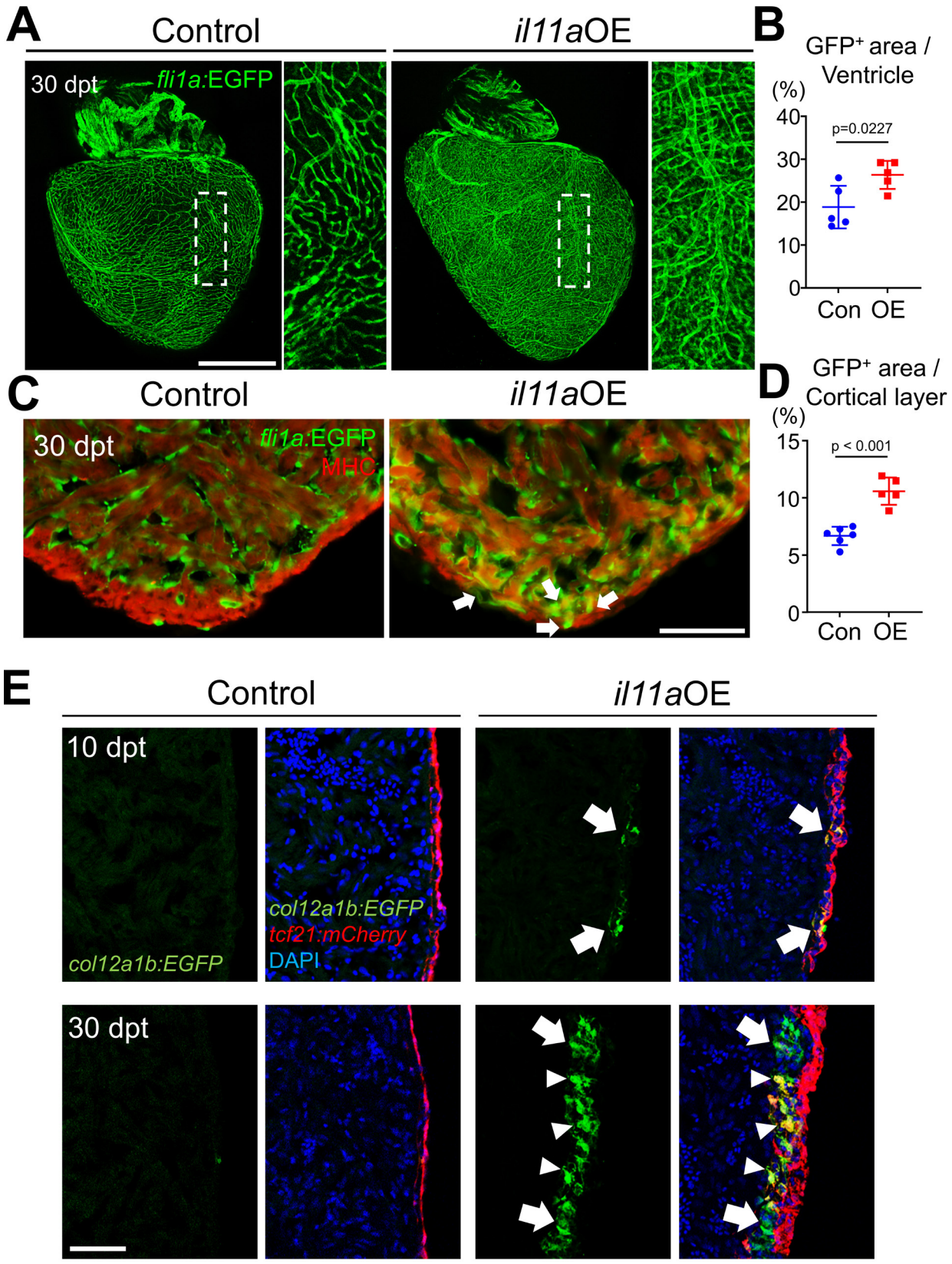
A
Control
il11aOE
30 dpt
fli1a:EGFP
B
GFP+ area / Ventricle
(%)
40
30
20
10
0
p=0.0227
Con
OE
C
Control
il11aOE
30 dpt
fli1a:EGFP
MHC
D
GFP+ area / Cortical layer
(%)
15
10
5
0
p < 0.001
Con
OE
E
Control
il11aOE
10 dpt
col12a1b:EGFP
col12a1b:EGFP
tcf21:mCherry
DAPI
30 dpt

Figure 3. *il11a* induction stimulates vascularization. (**A**) Representative whole-mount heart images from *fli1a:EGFP* control and *il11a*OE at 30 dpt. Insets correspond to higher magnifications of dashed boxes. (**B**) Quantification of *fli1a:EGFP*$^+$ vessel area in the ventricles for control (Con) and *il11a*OE (OE). n = 5. (**C**) Representative cardiac section images of control and *il11a*OE at 30 dpt. Green and red indicate *fli1a*:EGFP and myosin heavy chain (MHC), respectively. Arrows indicate expanded EGFP$^+$ region in the cortical layer. (**D**) Quantification of EGFP$^+$ area in the cortical muscle layer from control (Con) and *il11a*OE (OE). n = 5 - 6. (**E**) Representative cardiac section images of control and *il11a*OE expressing *tcf21:mCherry; col12a1b:EGFP.* Top, 10 dpt. Bottom, 30 dpt. Blue, DAPI. Green, EGFP. Red, mCherry. Arrows indicate *tcf21:mCherry* and *col12a1b:EGFP* double positive cells. Arrowheads indicate *tcf21:mCherry*$^-$*; col12a1b:EGFP*$^+$ cells. Scale bars, 500 μm in **A**, 50 μm in **C** and **E**.

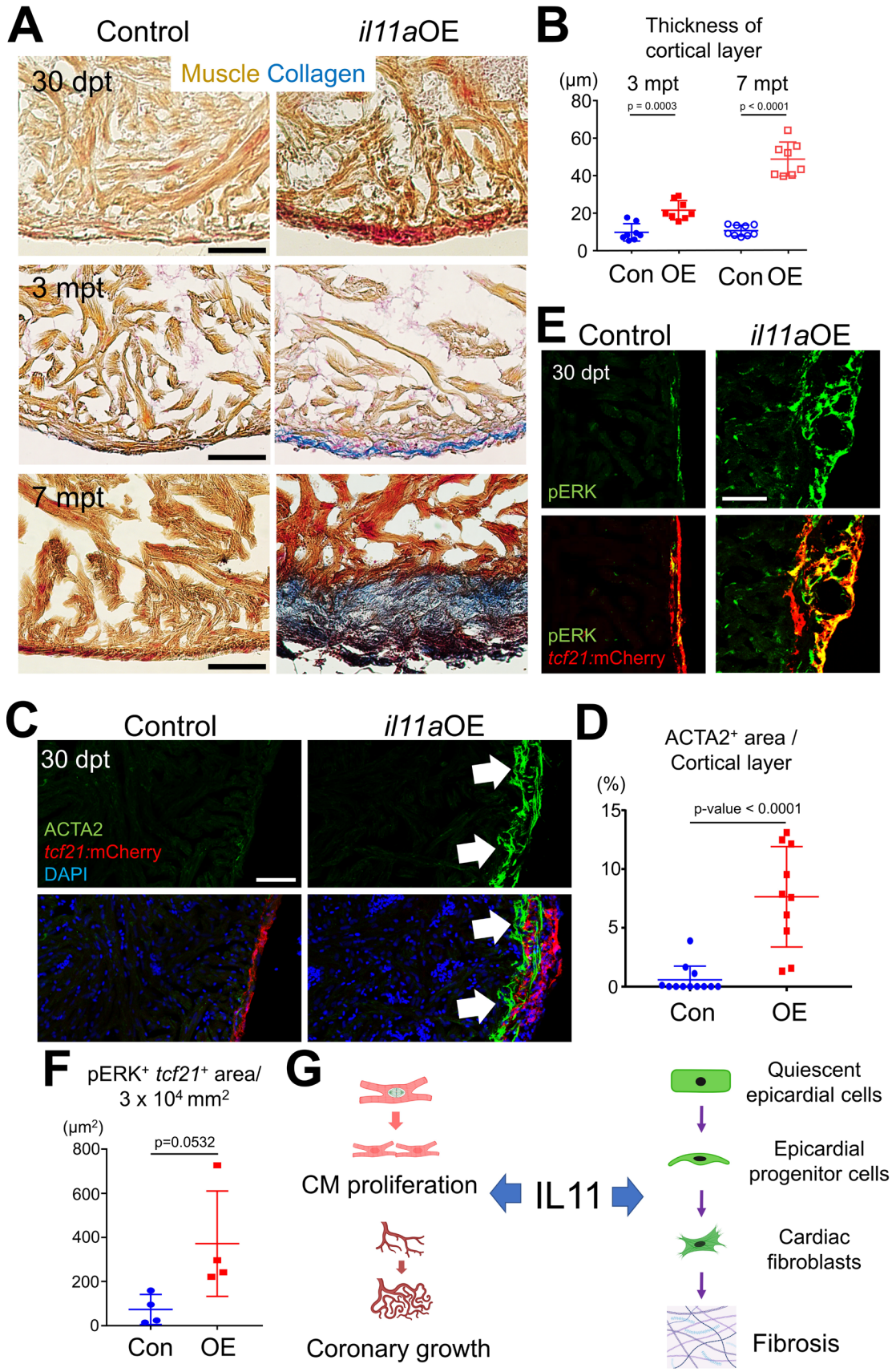
A
Control
il11aOE
30 dpt
Muscle Collagen
3 mpt
7 mpt
B
Thickness of cortical layer
(μm)
3 mpt
7 mpt
p = 0.0003
p < 0.0001
80
60
40
20
0
Con OE
Con OE
E
Control
il11aOE
30 dpt
pERK
pERK
tcf21:mCherry
C
Control
il11aOE
30 dpt
ACTA2
tcf21:mCherry
DAPI
D
ACTA2+ area / Cortical layer
(%)
p-value < 0.0001
15
10
5
0
Con
OE
F
pERK+ tcf21+ area/ 3 x 10^4 mm^2
(μm^2)
p=0.0532
800
600
400
200
0
Con
OE
G
CM proliferation
Coronary growth
IL11
Quiescent epicardial cells
Epicardial progenitor cells
Cardiac fibroblasts
Fibrosis

Figure 4. Fibrotic roles of *il11a* in adult zebrafish hearts. (**A**) Representative AFOG staining images of control and *il11a*OE uninjured hearts at 30 dpt (top), 3 mpt (middle), and 7 mpt (bottom). (**B**) Quantification of collagen$^+$ layer thickness in the ventricles from control (Con) and *il11a*OE (OE) at 3 and 7 mpt. n = 8 - 9. (**C**) Representative cardiac section images of control and *il11a*OE hearts at 30 dpt. Green and red indicate ACTA2$^+$ cardiac fibroblasts and *tcf21*$^+$ epicardium, respectively. Arrows represent ACTA2$^+$ cardiac fibroblasts. (**D**) Quantification of ACTA2$^+$ area in the cortical layer of the uninjured hearts between control (Con) and *il11a*OE (OE) at 30 dpt. n = 10 - 12. (**E**) Representative cardiac section images stained with mCherry (red) and pERK (green) of control and *il11a*OE hearts expressing *tcf21:mCherry* at 30 dpt. (**F**) Quantification of pERK$^+$ area in *tcf21*$^+$ epicardium in the ventricles for control (Con) and *il11a*OE (OE). n = 4. (**G**) Dual roles of IL11 in the hearts. IL11 triggers cardiac regeneration programs, including CM proliferation and revascularization. Simultaneously, IL11 contributes to fibrosis by stimulating quiescent epicardial cells to generate epicardial progenitor cells (EPCs), which give rise to cardiac fibroblasts. Scale bars, 25 μm (top and middle) and 50 μm (bottom) in **A**, 50 μm in **C** and **F**.

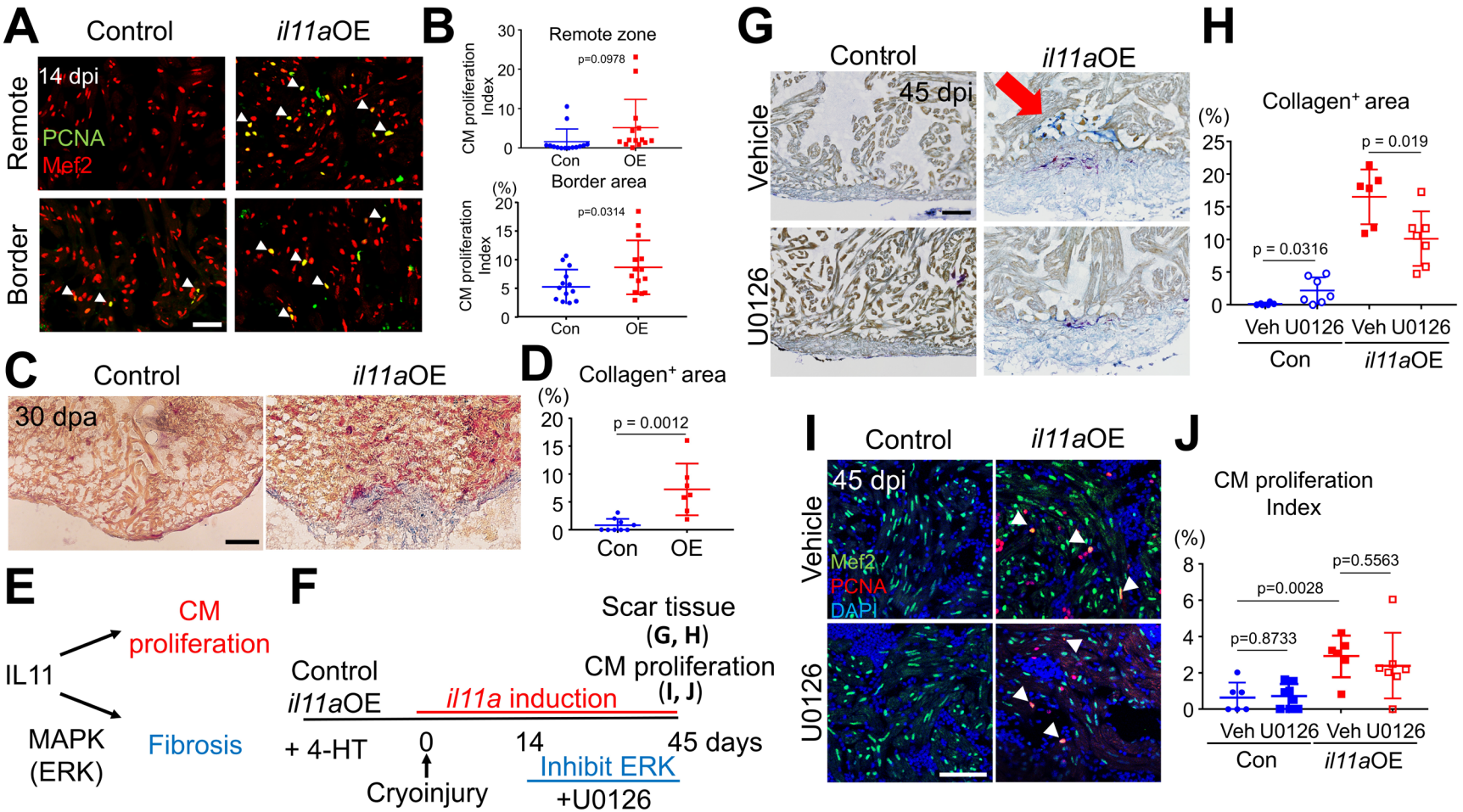
A
Control
il11aOE
Remote
Border
14 dpi
PCNA
Mef2
B
Remote zone
CM proliferation Index
p=0.0978
Con
OE
Border area
(%)
p=0.0314
C
Control
il11aOE
30 dpa
D
Collagen+ area
(%)
p = 0.0012
E
IL11
CM proliferation
MAPK (ERK)
Fibrosis
F
Control
il11aOE
il11a induction
+ 4-HT
0
14
45 days
Cryoinjury
Inhibit ERK
+U0126
Scar tissue (G, H)
CM proliferation (I, J)
G
Vehicle
U0126
45 dpi
H
Collagen+ area
p = 0.019
p = 0.0316
Veh U0126 Veh U0126
Con
il11aOE
I
Mef2
PCNA
DAPI
J
CM proliferation Index
p=0.5563
p=0.0028
p=0.8733

Figure 5. Combinatorial treatment enables to harness regenerative potential of *il11a* in the injured hearts. (**A**) Representative cardiac section images of control and *il11a*OE hearts stained with Mef2 (red) and PCNA (green) at 14 days post-injury (dpi). Cryoinjury was performed one day after administering four daily injection of 4-HT. Arrowheads indicate proliferative CMs. (**B**) CM proliferation index in the remote and border zone from control (Con) and *il11a*OE (OE) at 14 dpi. n = 14. (**C**) Representative AFOG staining images of control and *il11a*OE hearts at 30 dpa. (**D**) Quantification of collagen^{+} area in the ventricle of control (Con) and *il11a*OE (OE) at 30 dpa. n = 7 - 8. (**E**) Dual roles of *il11a* in injured hearts. *il11a* promotes CM proliferation while inducing fibrosis via Extracellular signal-regulated kinase (ERK) activity. (**F**) Experimental scheme to harness regenerative potential of *il11a* while mitigating fibrosis by treating U0126, an ERK inhibitor, starting at 14 dpi. (**G**) Representative AFOG staining images of vehicle (veh, 0.1% DMSO) or U0126 (10 μM) treated hearts from control and *il11a*OE. Hearts were collected at 45 dpi / 55 dpt. The arrow indicates the presence of scar tissue near the injury site in veh-treated *il11a*OE hearts. (**H**) Quantification of scar area in the ventricles of veh or U0126 treated control and *il11a*OE hearts. n = 6 - 7. (**I**) Representative cardiac section images of veh or U0126 treated control and *il11a*OE hearts stained with Mef2 (green) and PCNA (red) at 45 dpi. Arrowheads indicate proliferative CMs. (**J**) CM proliferation index in the ventricles of veh or U0126 treated control and *il11a*OE hearts at 45 dpi. n = 6 - 7. Scale bars, 25 μm in **A** and **G**, 50 μm in **C** and **I**.

Supplementary Figures

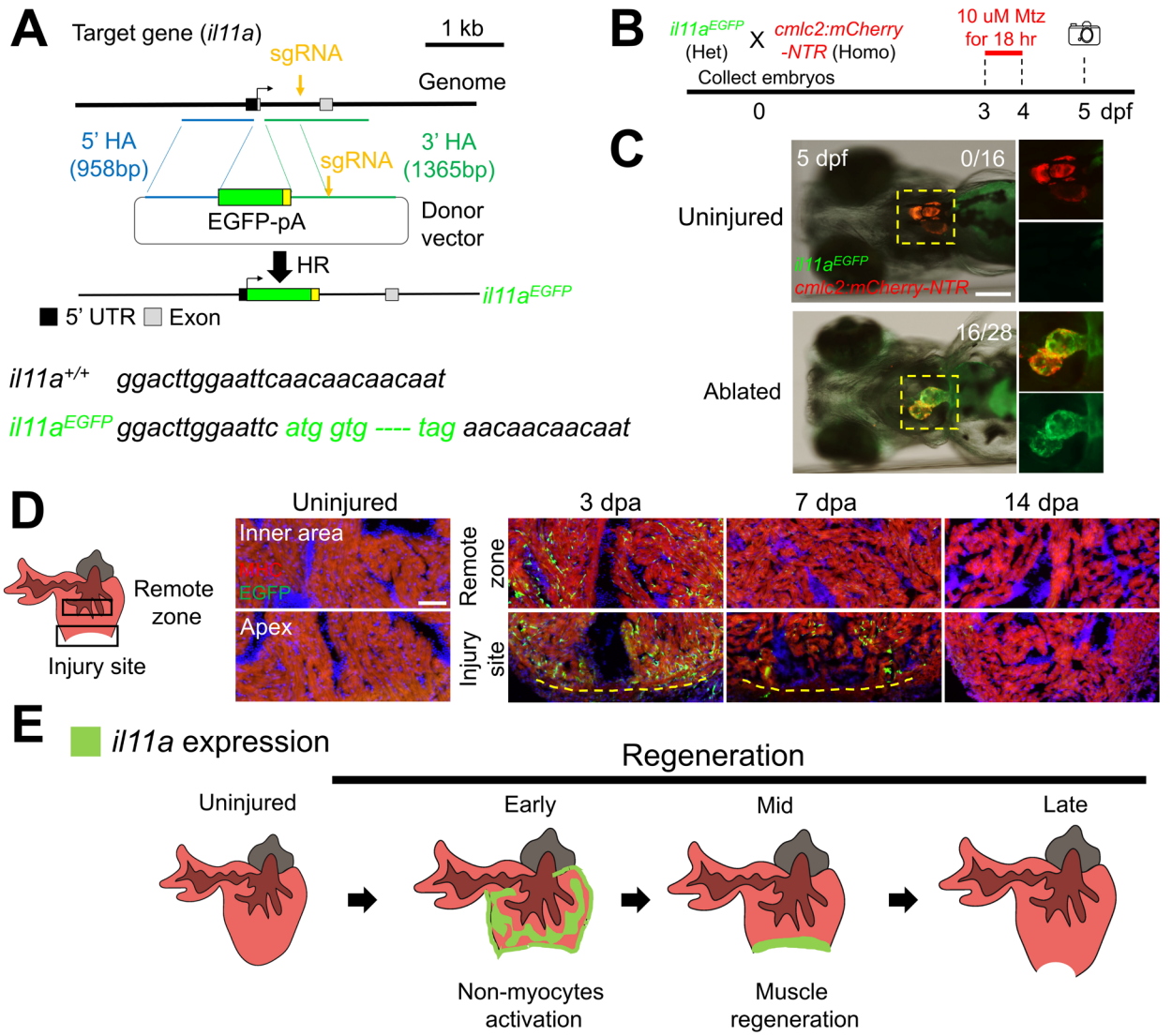

Figure S1. **Injury-inducible *il11a* expression in zebrafish hearts.** (**A**) Genomic structure of the endogenous *il11a* gene and the *il11a* knock-in reporter construct. sgRNA and a donor template together with Cas9 mRNA were injected into one-cell stage embryos to establish the *il11a*^{EGFP} knock-in reporter line. HA= Homology Arms, HR= Homologous Recombination. (**B**) The schematic to examine *il11a*^{EGFP} expression in larvae upon cardiac injury. Het, Heterozygote. Homo, Homozygote. (**C**) Representative images of uninjured and ablated hearts in *il11a*^{EGFP} larvae at 5 days-post fertilization (dpf).

Insets correspond to higher magnifications of dashed boxes. The number in the upper right corner of each image represents the fraction of the fish expressing EGFP. (**D**) Representative images of EGFP expression at the injury site and remote zone in *il11a*^{EGFP} hearts during heart regeneration. MHC (red) indicates myocardium. (**E**) Spatiotemporal expression and possible roles of *il11a*. *il11a* is strongly induced throughout the ventricle at the early stage of regeneration to activate non-cardiac muscle cells. At the intermediate stage, *il11a* expression is restricted to the wound area to promote CM proliferation. *il11a* expression returns to the basal level at the late stage of the regeneration. Scale bar, 100 μm in **C** and 50 μm in **D**.

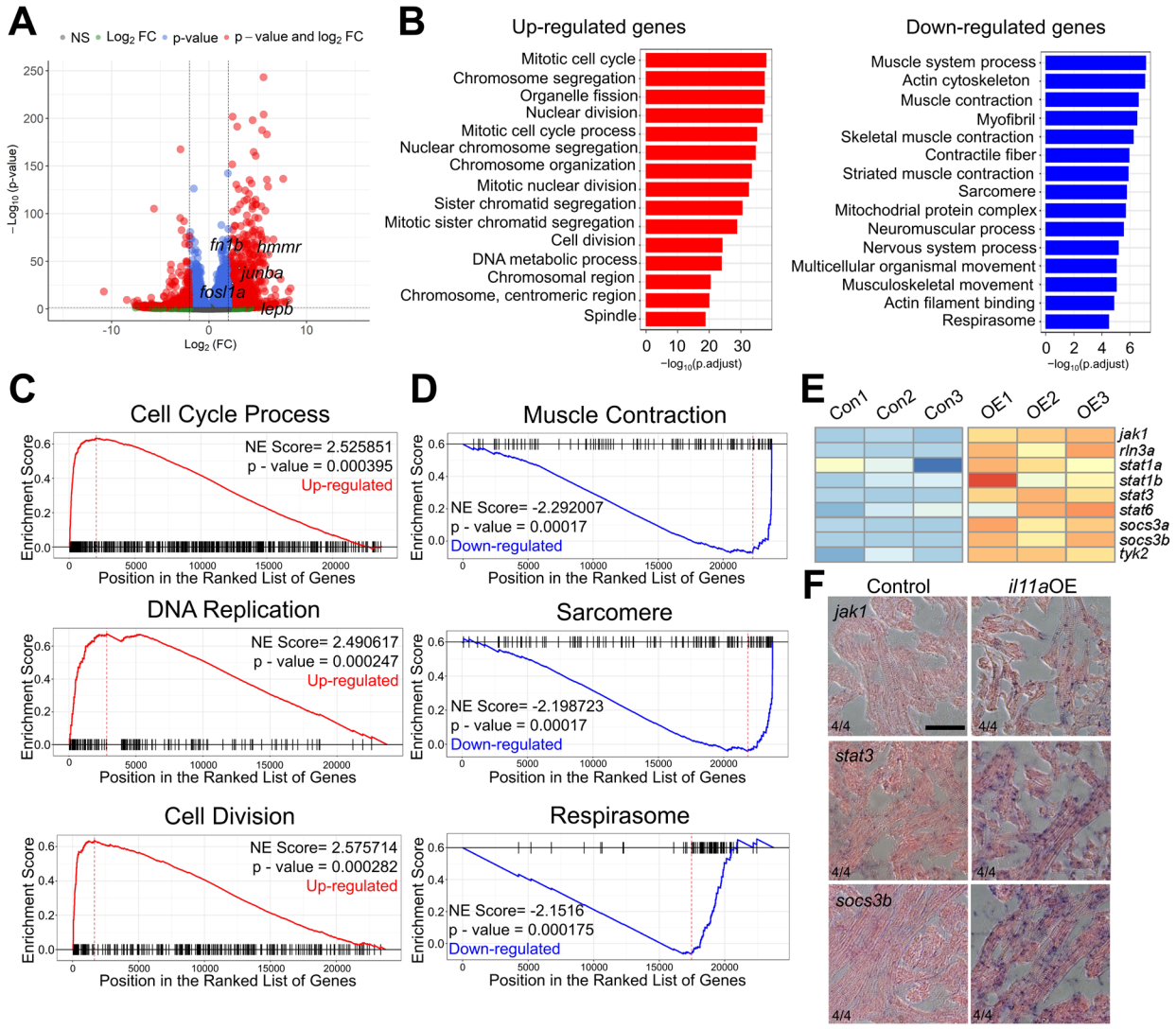

Figure S2. *il11a* OE triggers CM proliferation without the injury signal. (**A**) Differentially expressed genes between control and *il11a*OE ventricles shown as a volcano plot. Regeneration-associated genes, including *lepb, fn1b, hmmr, junba,* and *fosl1a*, are marked. (**B**) Gene ontology (GO) enrichment analysis of up- (left) and down- (right) regulated genes in the *il11a* OE. The bars indicate -$\log_{10}$(adjusted P-value). (**C, D**) Gene Set Enrichment Analysis (GSEA) plots of the up-regulated (**C**) and down-regulated (**D**) gene sets from control and *il11a*OE. *il11a*OE upregulates gene expression associated with cell cycle activity, DNA replication, and cell division, while downregulated genes are

associated with cardiac muscle contraction, sarcomere, and respirasome. (**E**) Heatmap of differentially expressed genes associated with JAK/STAT pathway for control and *il11a*OE. (**F**) Representative images of ISH (*in situ* hybridization) on cardiac sections of control and *il11a*OE. The number in the lower left corner of each image represents the fraction of the analyzed hearts with displayed phenotype. Scale bar, 20 μm in **F**.

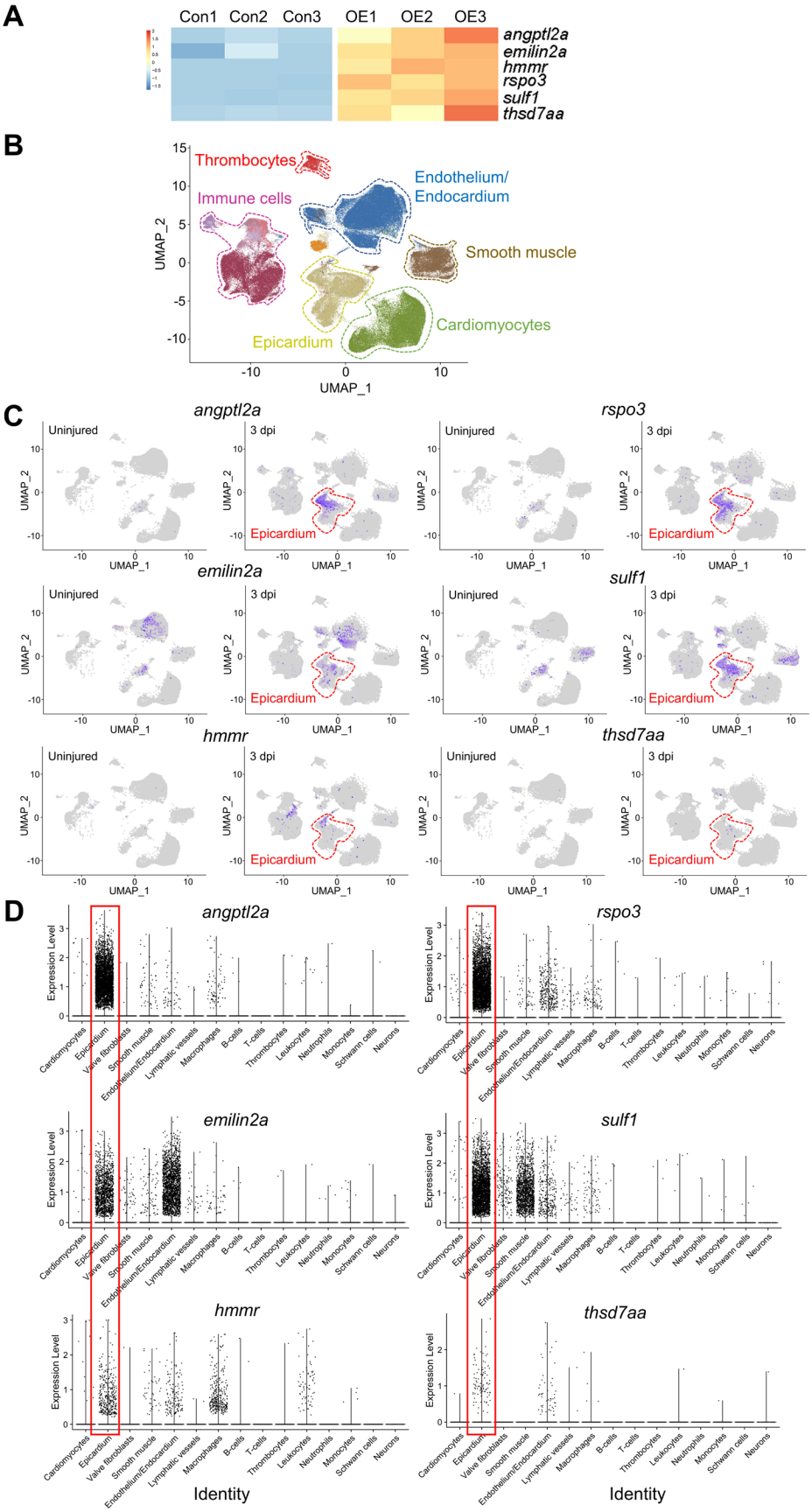
A
Con1
Con2
Con3
OE1
OE2
OE3
angptl2a
emilin2a
hmmr
rspo3
sulf1
thsd7aa
B
Thrombocytes
Immune cells
Endothelium/
Endocardium
Smooth muscle
Epicardium
Cardiomyocytes
UMAP_2
UMAP_1
C
angptl2a
rspo3
emilin2a
sulf1
hmmr
thsd7aa
Uninjured
3 dpi
Epicardium
D
Expression Level
Cardiomyocytes
Epicardium
Valve fibroblasts
Smooth muscle
Endothelium/Endocardium
Lymphatic vessels
Macrophages
B-cells
T-cells
Thrombocytes
Leukocytes
Neutrophils
Monocytes
Schwann cells
Neurons
Identity

Figure S3. *il11a*OE stimulates expression of epicardium-derived angiogenic factors. (**A**) Heatmap of differentially expressed genes responsible for vascularization from control and *il11a*OE. (**B**) Uniform manifold approximation and projection (UMAP) plot of regenerating zebrafish hearts and cell cluster analysis (**C**) Gene expression plots of angiogenic factor genes induced in the epicardium at 3 days post injury (dpi). (**D**) Violin plots showing expression of angiogenic factors in the cell populations of the hearts. Red boxes indicate the expression of the indicated genes in epicardium.

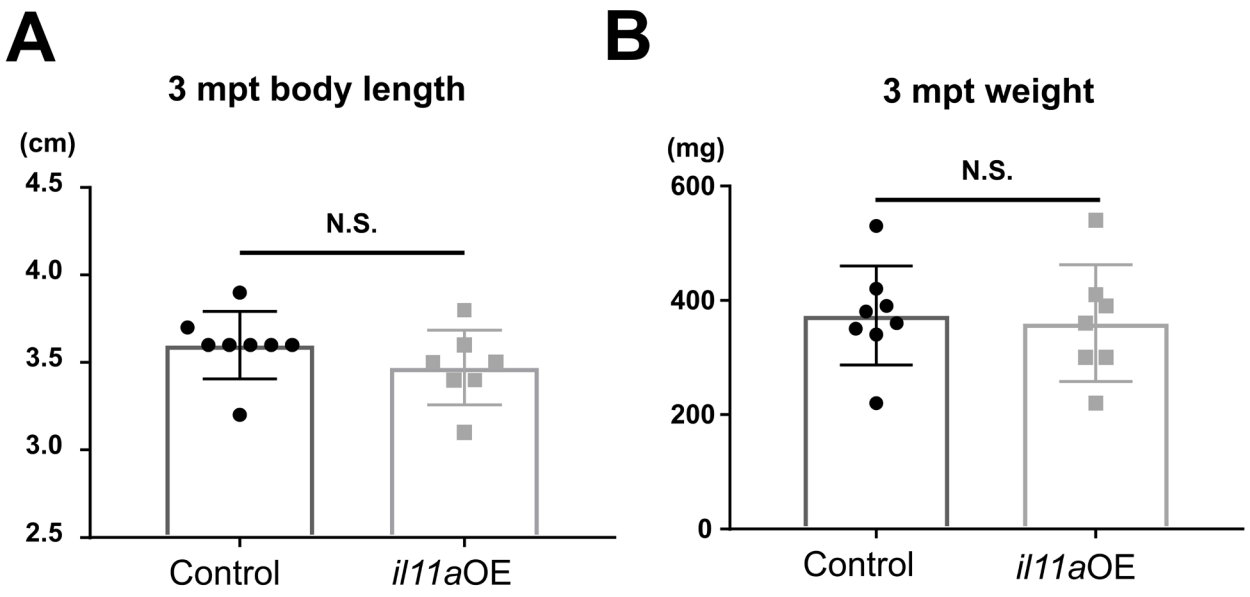

Figure S4. *il11a*OE adult fish have similar body length and weight to control. (**A, B**) The measurement of adult zebrafish body length (**A**) and body weight (**B**) 3 months after 4-HT treatment yielded no significant difference between control and *il11a*OE.

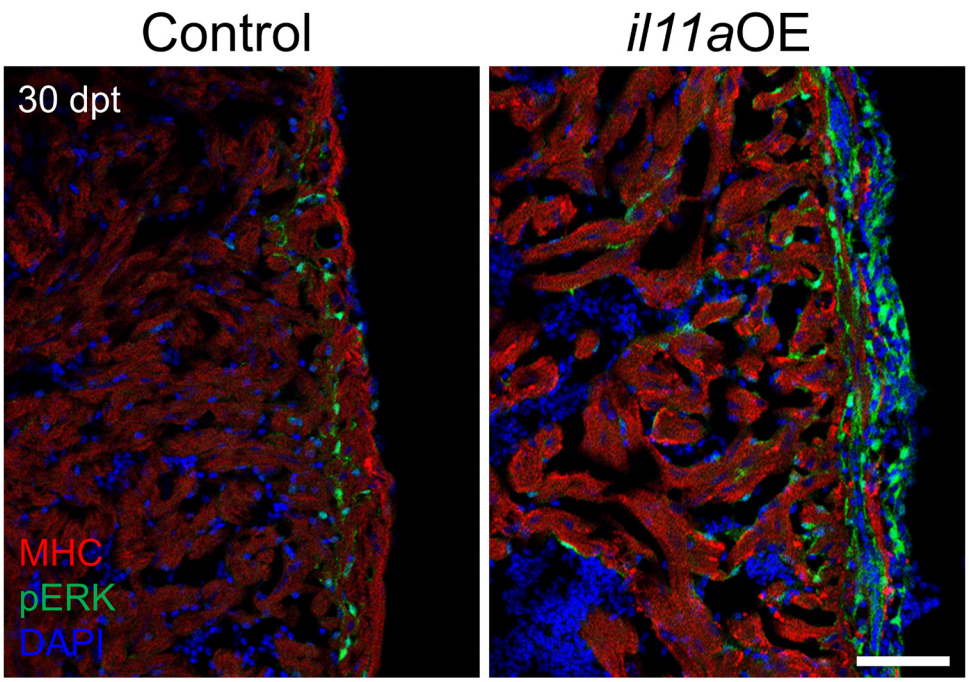

Figure S5. pERK signal is undetectable in CMs. Representative cardiac section images stained with myosin heavy chain (MHC, red) and pERK (green) from control and *il11a*OE at 30 dpt. pERK is significantly induced in ventricular wall, but not in MHC^{+} myocardium by *il11a*OE. Scale bar, 50 μm.

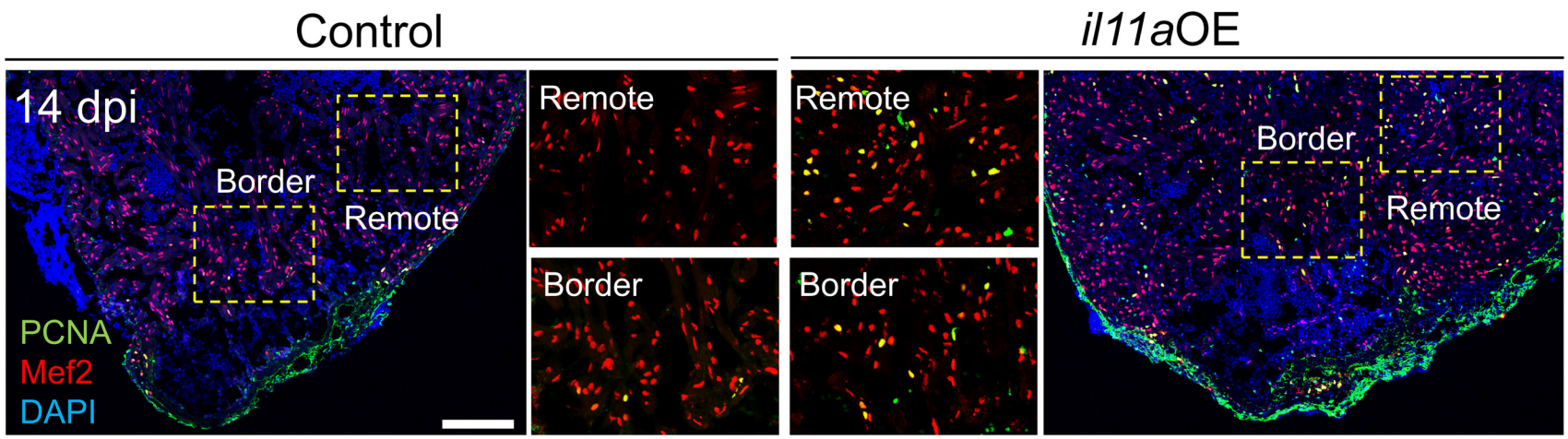

Figure S6. CM proliferation in the injured hearts is enhanced by *il11a* induction. Representative cardiac section images stained with Mef2 (red) and PCNA (green) from control and *il11a*OE following 4-HT treatment. dpi, days post-cryoinjury. Yellow dash boxes correspond to the region magnified in the border zone and remote area from control and *il11a*OE. Scale bar, 100 μm.

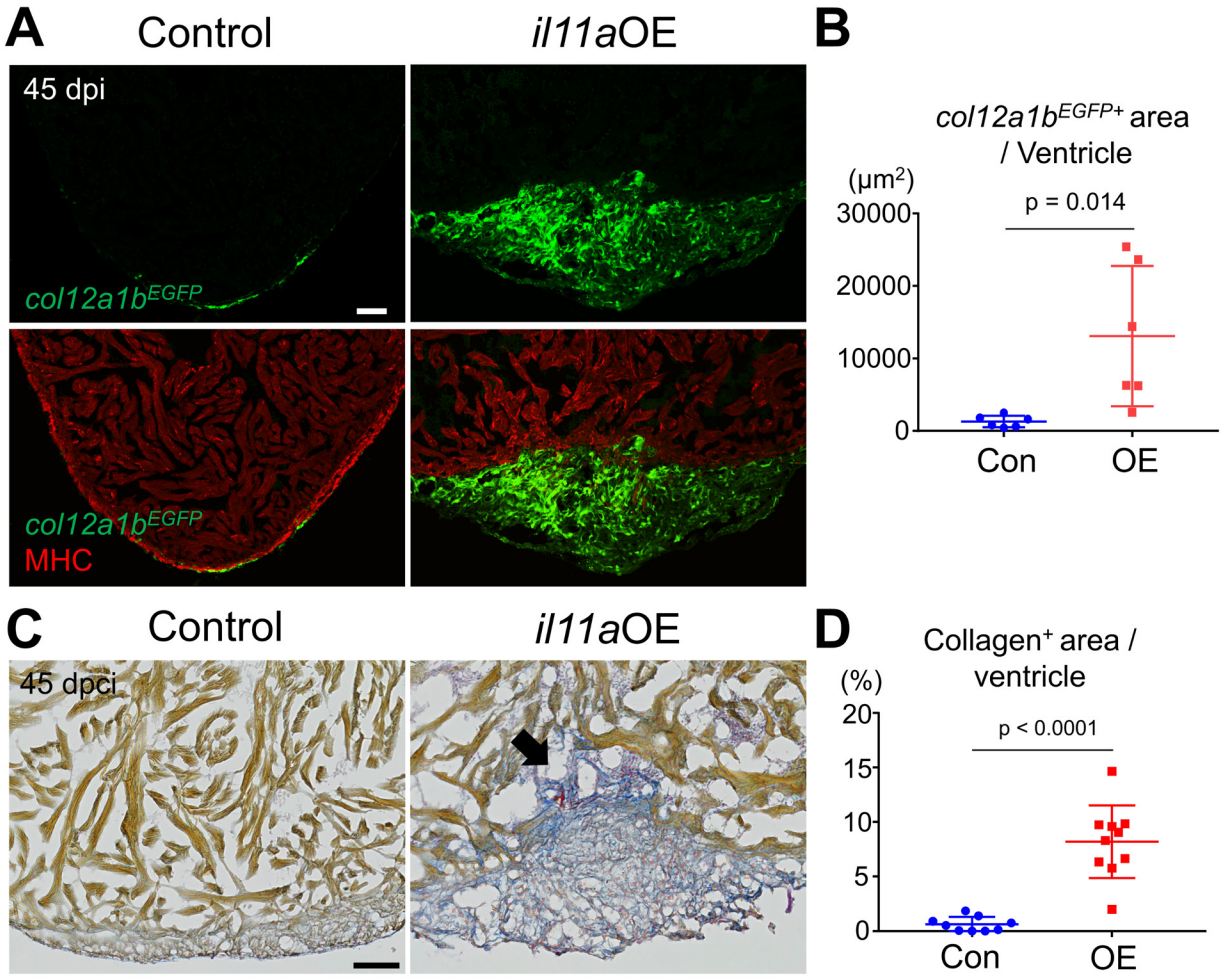

Figure S7. *il11a* induction in the injured hearts causes persistent EPC presence at the wound area, leading to collagen deposition at the wound area. (**A**) Representative cardiac section images of control and *il11a*OE expressing *col12a1b:EGFP* at 45 dpi. Green and red indicate *col12a1b:EGFP* and myosin heavy chain (MHC), respectively. (**B**) Quantification of EGFP$^+$ area at the injury site from control (Con) and *il11a*OE (OE). n = 6. (**C**) Representative AFOG staining images of control and *il11a*OE hearts at 60 days post-cryoinjury (dpci). (**D**) Quantification of collagen$^+$ area in the ventricle of control (Con) and *il11a*OE (OE) at 60 dpi. The arrow indicates the presence of scar tissue near the injury site. n = 9 - 10. Scale bars, 50μm in **A** and **C**.

Table S1. Primer list

il11a overexpression line generation	
il11a ATG XmaI -f	cga cccggg atgaaattgctgggtgactcctcc
il11a stop NotI -r	aac gcggccgc ctatttccccacaattcgaatc

il11a knock-in reporter line generation	
il11a 5' HM HindIII -f	cgg aagctt acagactgctgtctcaggac
il11a 5' HM EcoRI -r	gcc gaattc caagtccttgttttaaaaggt
il11a 3' HM NotI -f	tcc gcggccgc gctctgttatatttgtttacatttagt
il11a 3' HM KpnI -r	ctt ggtacc tgagtgctggatgtgagcacaa
il11a start GG-2 sgRNA template	GCG TAATACGACTCACTATA GG atc aagtg ttact cgctc GTTTTAGA GCTAGAAAtagc
3' universal primer	AAAGCACCGACTCGGTGCCACTTTTTCAAGTTGATAACG GACTAGCCTTATTTTAACTTGCTATTTCTAGCTCTAAAAC

In situ hybridization primers	
socs3b ISH -f	CTTTCTCCTGGAAGGATGGAGCA
socs3b ISH -r	TCAGTGAATAGCAGACGTCCTG
jak1 ISH -f	ACTCTGCTCAACTATTCTGTGCA
jak1 ISH -r	TGTCAAGCATCTGCTGAAAGTT
stat3 qPCR -f	TGGGTCGAGAAGGACATCA
stat3 ISH -r	TTTGGCTCGGAGAGAGAAAG

Supplementary Data 1. Table of differentially expressed genes in control and *il11a*OE hearts

References

1 Tzahor, E. & Dimmeler, S. A coalition to heal-the impact of the cardiac microenvironment. *Science* **377**, eabm4443, doi:10.1126/science.abm4443 (2022).

2 Schafer, S. *et al.* IL-11 is a crucial determinant of cardiovascular fibrosis. *Nature* **552**, 110-115, doi:10.1038/nature24676 (2017).

3 Lim, W. W. *et al.* Antibody-mediated neutralization of IL11 signalling reduces ERK activation and cardiac fibrosis in a mouse model of severe pressure overload. *Clinical and experimental pharmacology & physiology* **48**, 605-613, doi:10.1111/1440-1681.13458 (2021).

4 Corden, B., Adami, E., Sweeney, M., Schafer, S. & Cook, S. A. IL-11 in cardiac and renal fibrosis: Late to the party but a central player. *British journal of pharmacology* **177**, 1695-1708, doi:10.1111/bph.15013 (2020).

5 Poss, K. D., Wilson, L. G. & Keating, M. T. Heart regeneration in zebrafish. *Science* **298**, 2188-2190, doi:10.1126/science.1077857 (2002).

6 Mehdipour, M., Park, S. & Huang, G. N. Unlocking cardiomyocyte renewal potential for myocardial regeneration therapy. *Journal of molecular and cellular cardiology* **177**, 9-20, doi:10.1016/j.yjmcc.2023.02.002 (2023).

7 Jopling, C. *et al.* Zebrafish heart regeneration occurs by cardiomyocyte dedifferentiation and proliferation. *Nature* **464**, 606-609, doi:10.1038/nature08899 (2010).

8 Kikuchi, K. *et al.* Primary contribution to zebrafish heart regeneration by gata4(+) cardiomyocytes. *Nature* **464**, 601-605, doi:10.1038/nature08804 (2010).

9 Honkoop, H. *et al.* Single-cell analysis uncovers that metabolic reprogramming by ErbB2 signaling is essential for cardiomyocyte proliferation in the regenerating heart. *eLife* **8**, doi:10.7554/eLife.50163 (2019).

10 Wang, J. *et al.* The regenerative capacity of zebrafish reverses cardiac failure caused by genetic cardiomyocyte depletion. *Development* **138**, 3421-3430, doi:10.1242/dev.068601 (2011).

11 Munch, J., Grivas, D., Gonzalez-Rajal, A., Torregrosa-Carrion, R. & de la Pompa, J. L. Notch signalling restricts inflammation and serpine1 expression in the dynamic endocardium of the regenerating zebrafish heart. *Development* **144**, 1425-1440, doi:10.1242/dev.143362 (2017).

12 Sun, J., Peterson, E. A., Chen, X. & Wang, J. hapln1a(+) cells guide coronary growth during heart morphogenesis and regeneration. *Nat Commun* **14**, 3505, doi:10.1038/s41467-023-39323-6 (2023).

13 Zhao, L., Ben-Yair, R., Burns, C. E. & Burns, C. G. Endocardial Notch Signaling Promotes Cardiomyocyte Proliferation in the Regenerating Zebrafish Heart through Wnt Pathway Antagonism. *Cell Rep* **26**, 546-554 e545, doi:10.1016/j.celrep.2018.12.048 (2019).

14 Wei, K. H. *et al.* Comparative single-cell profiling reveals distinct cardiac resident macrophages essential for zebrafish heart regeneration. *eLife* **12**, doi:10.7554/eLife.84679 (2023).

15 Hui, S. P. *et al.* Zebrafish Regulatory T Cells Mediate Organ-Specific Regenerative Programs. *Developmental cell* **43**, 659-672 e655, doi:10.1016/j.devcel.2017.11.010 (2017).
16 Sanchez-Iranzo, H. *et al.* Transient fibrosis resolves via fibroblast inactivation in the regenerating zebrafish heart. *Proceedings of the National Academy of Sciences of the United States of America* **115**, 4188-4193, doi:10.1073/pnas.1716713115 (2018).
17 Kanisicak, O. *et al.* Genetic lineage tracing defines myofibroblast origin and function in the injured heart. *Nat Commun* **7**, 12260, doi:10.1038/ncomms12260 (2016).
18 Oka, T. *et al.* Genetic manipulation of periostin expression reveals a role in cardiac hypertrophy and ventricular remodeling. *Circulation research* **101**, 313-321, doi:10.1161/CIRCRESAHA.107.149047 (2007).
19 Gonzalez-Rosa, J. M., Martin, V., Peralta, M., Torres, M. & Mercader, N. Extensive scar formation and regression during heart regeneration after cryoinjury in zebrafish. *Development* **138**, 1663-1674, doi:10.1242/dev.060897 (2011).
20 de Bakker, D. E. M. *et al.* Prrx1b restricts fibrosis and promotes Nrg1-dependent cardiomyocyte proliferation during zebrafish heart regeneration. *Development* **148**, doi:10.1242/dev.198937 (2021).
21 Kirkiles-Smith, N. C. *et al.* IL-11 protects human microvascular endothelium from alloinjury in vivo by induction of survivin expression. *Journal of immunology* **172**, 1391-1396, doi:10.4049/jimmunol.172.3.1391 (2004).
22 Yu, J., Feng, Z., Tan, L., Pu, L. & Kong, L. Interleukin-11 protects mouse liver from warm ischemia/reperfusion (WI/Rp) injury. *Clin Res Hepatol Gastroenterol* **40**, 562-570, doi:10.1016/j.clinre.2015.11.009 (2016).
23 Tsujioka, H. *et al.* interleukin-11 induces and maintains progenitors of different cell lineages during Xenopus tadpole tail regeneration. *Nat Commun* **8**, 495, doi:10.1038/s41467-017-00594-5 (2017).
24 Allanki, S. *et al.* Interleukin-11 signaling promotes cellular reprogramming and limits fibrotic scarring during tissue regeneration. *Sci Adv* **7**, eabg6497, doi:10.1126/sciadv.abg6497 (2021).
25 Kang, J. *et al.* Modulation of tissue repair by regeneration enhancer elements. *Nature* **532**, 201-206, doi:10.1038/nature17644 (2016).
26 Wang, J., Karra, R., Dickson, A. L. & Poss, K. D. Fibronectin is deposited by injury-activated epicardial cells and is necessary for zebrafish heart regeneration. *Developmental biology* **382**, 427-435, doi:10.1016/j.ydbio.2013.08.012 (2013).
27 Missinato, M. A., Tobita, K., Romano, N., Carroll, J. A. & Tsang, M. Extracellular component hyaluronic acid and its receptor Hmmr are required for epicardial EMT during heart regeneration. *Cardiovascular research* **107**, 487-498, doi:10.1093/cvr/cvv190 (2015).
28 Beisaw, A. *et al.* AP-1 Contributes to Chromatin Accessibility to Promote Sarcomere Disassembly and Cardiomyocyte Protrusion during Zebrafish Heart Regeneration. *Circulation research*, doi:10.1161/CIRCRESAHA.119.316167 (2020).
29 Johnstone, C. N., Chand, A., Putoczki, T. L. & Ernst, M. Emerging roles for IL-11 signaling in cancer development and progression: Focus on breast cancer.

Cytokine Growth Factor Rev **26**, 489-498, doi:10.1016/j.cytogfr.2015.07.015 (2015).

30 Obana, M. *et al.* Therapeutic activation of signal transducer and activator of transcription 3 by interleukin-11 ameliorates cardiac fibrosis after myocardial infarction. *Circulation* **121**, 684-691, doi:10.1161/CIRCULATIONAHA.109.893677 (2010).

31 Fang, Y. *et al.* Translational profiling of cardiomyocytes identifies an early Jak1/Stat3 injury response required for zebrafish heart regeneration. *Proceedings of the National Academy of Sciences of the United States of America* **110**, 13416-13421, doi:10.1073/pnas.1309810110 (2013).

32 Ogawa, M. *et al.* Kruppel-like factor 1 is a core cardiomyogenic trigger in zebrafish. *Science* **372**, 201-205, doi:10.1126/science.abe2762 (2021).

33 Porrello, E. R. *et al.* Transient regenerative potential of the neonatal mouse heart. *Science* **331**, 1078-1080, doi:10.1126/science.1200708 (2011).

34 D'Uva, G. *et al.* ERBB2 triggers mammalian heart regeneration by promoting cardiomyocyte dedifferentiation and proliferation. *Nature cell biology* **17**, 627-638, doi:10.1038/ncb3149 (2015).

35 Vasan, R. S., Larson, M. G., Benjamin, E. J., Evans, J. C. & Levy, D. Left ventricular dilatation and the risk of congestive heart failure in people without myocardial infarction. *N Engl J Med* **336**, 1350-1355, doi:10.1056/NEJM199705083361903 (1997).

36 Marin-Juez, R. *et al.* Fast revascularization of the injured area is essential to support zebrafish heart regeneration. *Proceedings of the National Academy of Sciences of the United States of America* **113**, 11237-11242, doi:10.1073/pnas.1605431113 (2016).

37 Marin-Juez, R. *et al.* Coronary Revascularization During Heart Regeneration Is Regulated by Epicardial and Endocardial Cues and Forms a Scaffold for Cardiomyocyte Repopulation. *Developmental cell* **51**, 503-515 e504, doi:10.1016/j.devcel.2019.10.019 (2019).

38 Das, S. *et al.* A Unique Collateral Artery Development Program Promotes Neonatal Heart Regeneration. *Cell* **176**, 1128-1142 e1118, doi:10.1016/j.cell.2018.12.023 (2019).

39 Harrison, M. R. *et al.* Chemokine-guided angiogenesis directs coronary vasculature formation in zebrafish. *Developmental cell* **33**, 442-454, doi:10.1016/j.devcel.2015.04.001 (2015).

40 Harrison, M. R. *et al.* Late developing cardiac lymphatic vasculature supports adult zebrafish heart function and regeneration. *eLife* **8**, doi:10.7554/eLife.42762 (2019).

41 El-Sammak, H. *et al.* A Vegfc-Emilin2a-Cxcl8a Signaling Axis Required for Zebrafish Cardiac Regeneration. *Circulation research* **130**, 1014-1029, doi:10.1161/CIRCRESAHA.121.319929 (2022).

42 Korf-Klingebiel, M. *et al.* Heparan Sulfate-Editing Extracellular Sulfatases Enhance VEGF Bioavailability for Ischemic Heart Repair. *Circulation research* **125**, 787-801, doi:10.1161/CIRCRESAHA.119.315023 (2019).

43 Scholz, B. *et al.* Endothelial RSPO3 Controls Vascular Stability and Pruning through Non-canonical WNT/Ca(2+)/NFAT Signaling. *Developmental cell* **36**, 79-93, doi:10.1016/j.devcel.2015.12.015 (2016).

44 Hu, B. *et al.* Origin and function of activated fibroblast states during zebrafish heart regeneration. *Nature genetics* **54**, 1227-1237, doi:10.1038/s41588-022-01129-5 (2022).
45 Liu, L. Y. *et al.* Motor neuron-derived Thsd7a is essential for zebrafish vascular development via the Notch-dll4 signaling pathway. *J Biomed Sci* **23**, 59, doi:10.1186/s12929-016-0277-9 (2016).
46 Zhou, B. *et al.* Adult mouse epicardium modulates myocardial injury by secreting paracrine factors. *J Clin Invest* **121**, 1894-1904, doi:10.1172/JCI45529 (2011).
47 Quijada, P., Trembley, M. A. & Small, E. M. The Role of the Epicardium During Heart Development and Repair. *Circulation research* **126**, 377-394, doi:10.1161/CIRCRESAHA.119.315857 (2020).
48 Cao, J. & Poss, K. D. The epicardium as a hub for heart regeneration. *Nat Rev Cardiol*, doi:10.1038/s41569-018-0046-4 (2018).
49 Xia, Y. *et al.* Activation of a transient progenitor state in the epicardium is required for zebrafish heart regeneration. *Nat Commun* **13**, 7704, doi:10.1038/s41467-022-35433-9 (2022).
50 Gonzalez-Rosa, J. M., Peralta, M. & Mercader, N. Pan-epicardial lineage tracing reveals that epicardium derived cells give rise to myofibroblasts and perivascular cells during zebrafish heart regeneration. *Developmental biology* **370**, 173-186, doi:10.1016/j.ydbio.2012.07.007 (2012).
51 Peralta, M., Gonzalez-Rosa, J. M., Marques, I. J. & Mercader, N. The Epicardium in the Embryonic and Adult Zebrafish. *J Dev Biol* **2**, 101-116, doi:10.3390/jdb2020101 (2014).
52 Lavoie, H., Gagnon, J. & Therrien, M. ERK signalling: a master regulator of cell behaviour, life and fate. *Nature reviews. Molecular cell biology* **21**, 607-632, doi:10.1038/s41580-020-0255-7 (2020).
53 Foglia, B., Cannito, S., Bocca, C., Parola, M. & Novo, E. ERK Pathway in Activated, Myofibroblast-Like, Hepatic Stellate Cells: A Critical Signaling Crossroad Sustaining Liver Fibrosis. *Int J Mol Sci* **20**, doi:10.3390/ijms20112700 (2019).
54 Favata, M. F. *et al.* Identification of a novel inhibitor of mitogen-activated protein kinase kinase. *The Journal of biological chemistry* **273**, 18623-18632, doi:10.1074/jbc.273.29.18623 (1998).
55 Cohen, O. & Granek, R. Nucleus-targeted drug delivery: theoretical optimization of nanoparticles decoration for enhanced intracellular active transport. *Nano Lett* **14**, 2515-2521, doi:10.1021/nl500248q (2014).
56 Fu, A., Tang, R., Hardie, J., Farkas, M. E. & Rotello, V. M. Promises and pitfalls of intracellular delivery of proteins. *Bioconjug Chem* **25**, 1602-1608, doi:10.1021/bc500320j (2014).
57 Shaw, S., Sarkar, A. K. & Jana, N. R. Protein Delivery to the Cytosol and Cell Nucleus via Micellar Nanocarrier-Based Nonendocytic Uptake. *ACS Appl Bio Mater*, doi:10.1021/acsabm.3c00431 (2023).
58 Travers, J. G., Kamal, F. A., Robbins, J., Yutzey, K. E. & Blaxall, B. C. Cardiac Fibrosis: The Fibroblast Awakens. *Circulation research* **118**, 1021-1040, doi:10.1161/CIRCRESAHA.115.306565 (2016).

59 Gonzalez-Rosa, J. M., Burns, C. E. & Burns, C. G. Zebrafish heart regeneration: 15 years of discoveries. *Regeneration (Oxf)* **4**, 105-123, doi:10.1002/reg2.83 (2017).
60 Ross Stewart, K. M., Walker, S. L., Baker, A. H., Riley, P. R. & Brittan, M. Hooked on heart regeneration: the zebrafish guide to recovery. *Cardiovascular research* **118**, 1667-1679, doi:10.1093/cvr/cvab214 (2022).
61 Csobonyeiova, M., Beerova, N., Klein, M., Debreova-Cehakova, M. & Danisovic, L. Cell-Based and Selected Cell-Free Therapies for Myocardial Infarction: How Do They Compare to the Current Treatment Options? *Int J Mol Sci* **23**, doi:10.3390/ijms231810314 (2022).
62 Hashimoto, H., Olson, E. N. & Bassel-Duby, R. Therapeutic approaches for cardiac regeneration and repair. *Nat Rev Cardiol* **15**, 585-600, doi:10.1038/s41569-018-0036-6 (2018).
63 Trepicchio, W. L., Bozza, M., Bouchard, P. & Dorner, A. J. Protective effect of rhIL-11 in a murine model of acetaminophen-induced hepatotoxicity. *Toxicol Pathol* **29**, 242-249, doi:10.1080/019262301317052521 (2001).
64 Zhao, X. F. *et al.* Leptin and IL-6 family cytokines synergize to stimulate Muller glia reprogramming and retina regeneration. *Cell Rep* **9**, 272-284, doi:10.1016/j.celrep.2014.08.047 (2014).
65 Ng, B. *et al.* Interleukin-11 is a therapeutic target in idiopathic pulmonary fibrosis. *Science translational medicine* **11**, doi:10.1126/scitranslmed.aaw1237 (2019).
66 Yang, W. *et al.* Interleukin-11 regulates the fate of adipose-derived mesenchymal stem cells via STAT3 signalling pathways. *Cell Prolif* **53**, e12771, doi:10.1111/cpr.12771 (2020).
67 Kimura, R. *et al.* Identification of cardiac myocytes as the target of interleukin 11, a cardioprotective cytokine. *Cytokine* **38**, 107-115, doi:10.1016/j.cyto.2007.05.011 (2007).
68 Chen, C. H., Durand, E., Wang, J., Zon, L. I. & Poss, K. D. zebraflash transgenic lines for in vivo bioluminescence imaging of stem cells and regeneration in adult zebrafish. *Development* **140**, 4988-4997, doi:10.1242/dev.102053 (2013).
69 Lawson, N. D. & Weinstein, B. M. In vivo imaging of embryonic vascular development using transgenic zebrafish. *Developmental biology* **248**, 307-318 (2002).
70 Proulx, K., Lu, A. & Sumanas, S. Cranial vasculature in zebrafish forms by angioblast cluster-derived angiogenesis. *Developmental biology* **348**, 34-46, doi:10.1016/j.ydbio.2010.08.036 (2010).
71 Wang, J., Cao, J., Dickson, A. L. & Poss, K. D. Epicardial regeneration is guided by cardiac outflow tract and Hedgehog signalling. *Nature* **522**, 226-230, doi:10.1038/nature14325 (2015).
72 Gemberling, M., Karra, R., Dickson, A. L. & Poss, K. D. Nrg1 is an injury-induced cardiomyocyte mitogen for the endogenous heart regeneration program in zebrafish. *eLife* **4**, doi:10.7554/eLife.05871 (2015).
73 Chablais, F. & Jazwinska, A. Induction of myocardial infarction in adult zebrafish using cryoinjury. *J Vis Exp*, doi:10.3791/3666 (2012).

74 Keating, M. *et al.* A robust knock-in approach using a minimal promoter and a minicircle. *bioRxiv*, 2023.2009.2015.558008, doi:10.1101/2023.09.15.558008 (2023).
75 Sehring, I. *et al.* Zebrafish fin regeneration involves generic and regeneration-specific osteoblast injury responses. *eLife* **11**, doi:10.7554/eLife.77614 (2022).
76 Begeman, I. J. *et al.* Decoding an organ regeneration switch by dissecting cardiac regeneration enhancers. *Development* **147**, doi:10.1242/dev.194019 (2020).
77 Patra, C. *et al.* The zebrafish ventricle: A hub of cardiac endothelial cells for in vitro cell behavior studies. *Sci Rep* **7**, 2687, doi:10.1038/s41598-017-02461-1 (2017).
78 Kim, D., Paggi, J. M., Park, C., Bennett, C. & Salzberg, S. L. Graph-based genome alignment and genotyping with HISAT2 and HISAT-genotype. *Nature biotechnology* **37**, 907-915, doi:10.1038/s41587-019-0201-4 (2019).
79 Liao, Y., Smyth, G. K. & Shi, W. featureCounts: an efficient general purpose program for assigning sequence reads to genomic features. *Bioinformatics* **30**, 923-930, doi:10.1093/bioinformatics/btt656 (2014).
80 Love, M. I., Huber, W. & Anders, S. Moderated estimation of fold change and dispersion for RNA-seq data with DESeq2. *Genome biology* **15**, 550, doi:10.1186/s13059-014-0550-8 (2014).
81 Wu, T. *et al.* clusterProfiler 4.0: A universal enrichment tool for interpreting omics data. *Innovation (N Y)* **2**, 100141, doi:10.1016/j.xinn.2021.100141 (2021).
82 Rao, A. *et al.* The translation initiation factor homolog eif4e1c regulates cardiomyocyte metabolism and proliferation during heart regeneration. *Development* **150**, doi:10.1242/dev.201376 (2023).
83 Stuart, T. *et al.* Comprehensive Integration of Single-Cell Data. *Cell* **177**, 1888-1902 e1821, doi:10.1016/j.cell.2019.05.031 (2019).